


## RESEARCH ARTICLE OPEN ACCESS

# Neuid: A Novel Neuron-Enriched LncRNA that Connects Epigenetic Gene Silencing to Alzheimer's Disease

Ranjit Pradhan<sup>1</sup> | Zorica Petrovic<sup>2</sup> | M. Sadman Sakib<sup>1</sup> | Sophie Schröder<sup>1</sup> | Dennis Manfred Krüger<sup>1,3</sup> | Tonatiuh Pena<sup>1,3</sup> | Eren Diniz<sup>1</sup> | Susanne Burkhardt<sup>1</sup> | Anna-Lena Schütz<sup>4</sup> | Verena Gisa<sup>1</sup> | Iga Grzadzielewska<sup>1</sup> | Karl Toischer<sup>5,6,7</sup> | Thor D. Stein<sup>8,9,10,11</sup> | Jan Krzysztof Blusztajn<sup>8,11</sup> | Ivana Delalle<sup>8,11</sup> | Jelena Radulovic<sup>12,13</sup> | Farahnaz Sananbenesi<sup>3,4</sup> | Andre Fischer<sup>5,6,14</sup> 

<sup>1</sup>Department For Epigenetics and Systems Medicine in Neurodegenerative Diseases, German Center for Neurodegenerative Diseases (DZNE), Göttingen, Germany | <sup>2</sup>Dominick P. Purpura Department of Neuroscience, Albert Einstein College of Medicine, Bronx, New York, USA | <sup>3</sup>Bioinformatics Unit, German Center for Neurodegenerative Diseases (DZNE), Göttingen, Germany | <sup>4</sup>Research Group for Genome Dynamics in Brain Diseases, German Center for Neurodegenerative Diseases, Göttingen, Germany | <sup>5</sup>Cluster of Excellence "Multiscale Bioimaging: from Molecular Machines to Networks of Excitable Cells" (MBExC), University of Göttingen, Göttingen, Germany | <sup>6</sup>German Center for Cardiovascular Diseases (DZKH), Göttingen, Germany | <sup>7</sup>Department of Cardiology and Pneumology, Georg-August-University, Goettingen, Germany | <sup>8</sup>Department of Pathology and Laboratory Medicine, Boston University Chobanian and Avedisian School of Medicine, Boston, Massachusetts, USA | <sup>9</sup>VA Boston Healthcare System, Boston, Massachusetts, USA | <sup>10</sup>Department of Veterans Affairs Medical Center, Bedford, Massachusetts, USA | <sup>11</sup>Boston University Alzheimer's Disease Research Center, Boston University Chobanian and Avedisian School of Medicine, Boston, Massachusetts, USA | <sup>12</sup>Department of Biomedicine, Aarhus University, PROMEMO, DANDRITE, Aarhus University, Aarhus, Denmark | <sup>13</sup>Dominick P. Purpura Department of Neuroscience and Department of Psychiatry and Behavioral Sciences, Psychiatry Research Institute Montefiore Einstein (PRIME), Albert Einstein College of Medicine, Bronx, New York, USA | <sup>14</sup>Department For Psychiatry and Psychotherapy, University Medical Center of Göttingen, Georg-August University, Göttingen, Germany

**Correspondence:** Andre Fischer ([andre.fischer@dzne.de](mailto:andre.fischer@dzne.de))

**Received:** 6 August 2025 | **Revised:** 2 February 2026 | **Accepted:** 6 March 2026

**Keywords:** brain | epigenetics | long-non-coding RNA | neurodegeneration | non-coding RNA

## ABSTRACT

The increasing evidence that non-coding RNAs can become deregulated during pathogenesis is dramatically expanding the space for drug discovery beyond the protein-coding genome. Long noncoding RNAs (lncRNAs) are emerging as key regulators of cellular function, yet most remain uncharacterized. Here, we identify a previously unstudied lncRNA, which we named Neuronal Identity (*Neuid*), a conserved, brain-enriched transcript expressed in neurons. *Neuid* is downregulated in the brains of Alzheimer's disease (AD) patients. Mechanistically, *Neuid* maintains neuronal identity by repressing developmental and glial genes via interaction with the PRC2 subunit EZH2 and regulation of H3K27me3. Knockdown of *Neuid* disrupts this repression, leading to impaired neuronal activity and memory formation. Importantly, CRISPRa-mediated *Neuid* overexpression restores neuronal function in A $\beta$ 42-treated neurons. These findings identify *Neuid* as a critical regulator of neuronal plasticity and position it as a promising therapeutic target for AD

## 1 | Introduction

Basic and translational research over the past decades has primarily focused on the protein-coding portion of the genome, that is the ~1.5% of genes translated into proteins and targeted

by small molecules or biologics. In contrast, the vast majority of the genome is transcribed into non-coding RNAs (ncRNAs), including a substantial group known as long non-coding RNAs (lncRNAs), which are defined as transcripts longer than 300 nucleotides without protein-coding potential [1, 2]. Initially

This is an open access article under the terms of the [Creative Commons Attribution](https://creativecommons.org/licenses/by/4.0/) License, which permits use, distribution and reproduction in any medium, provided the original work is properly cited.

© 2026 The Author(s). *Advanced Science* published by Wiley-VCH GmbH

dismissed as transcriptional noise, lncRNAs are now recognized as functional molecules involved in diverse biological processes [3, 4].

Many lncRNAs exhibit tissue- and cell type-specific expression patterns, with approximately 40% reported to be brain-specific [5]. This suggests that lncRNAs play key roles not only in brain development and function, but potentially also in the pathogenesis of brain disorders [6–11]. The analysis of lncRNAs in brain disease is therefore greatly expanding the landscape for drug discovery. In particular, neurodegenerative disease-associated lncRNAs that are selectively enriched in neurons may represent promising targets for therapeutic intervention, as their brain- and cell type-specific expression suggests the potential for high specificity with minimal side effects.

These properties, alongside advances in RNA-based therapies, make lncRNAs attractive candidates for targeted drug development [12, 13].

Despite their promise, our understanding of lncRNAs in the brain, especially in the context of neurodegenerative diseases such as Alzheimer's disease (AD), remains limited [14–16].

AD is the most prevalent neurodegenerative disorder in the elderly and is believed to follow a specific sequence of pathological events that can be distinguished into different phases. While not undisputed, it is widely believed to begin with the accumulation of amyloid beta peptides, followed by aggregation of the Tau protein and deregulation of glial cells, eventually leading to loss of neuronal homeostasis and neuronal death [17, 18]. Current therapeutic approaches focus on drugs that affect amyloid beta and Tau aggregation or modulate glial cell functions such as microglia-mediated neuroinflammation [19–21]. However, AD is a multifactorial disease, and effective treatment will likely require combinatorial therapies using multiple approaches tailored to the patient's disease stage [22].

On this basis, and in light of the emerging promise of RNA therapeutics for a wide range of diseases, we propose that a deeper understanding of lncRNAs in neuronal function can help develop precision therapeutic approaches to treat neurodegenerative diseases such as AD [13, 23, 24].

In this study, we systematically identified lncRNAs that fulfil these criteria. Using integrated OMICS datasets from humans and mice, we discovered a previously uncharacterized lncRNA, which we named *Neuronal Identity lncRNA (Neuid)*. In mice and humans *Neuid* is almost exclusively expressed in neurons. Its expression is consistently reduced in the brains of AD patients and in cultured neurons exposed to A $\beta$ 42. Mechanistically, *Neuid* represses non-neuronal gene expression via the Polycomb Repressive Complex 2 (PRC2), which mediates transcriptional silencing through trimethylation of lysine 27 on histone H3 (H3K27me3). *Neuid* loss impairs neuronal plasticity and memory, while CRISPRa-mediated upregulation of *Neuid* restores network function in A $\beta$ 42-treated neurons.

In conclusion, our findings validate the feasibility of a systematic approach to identify lncRNAs as therapeutic targets in AD and

highlight *Neuid* as a promising candidate for future RNA-based neuroprotective strategies.

## 2 | Methods

### 2.1 | Human Tissues

For the analysis of *NEUID* expression by qPCR, brains (prefrontal cortex, BA9) from control ( $n = 2$  females & 2 males; age =  $81.75 \pm 7.41$  years, PMD =  $13.75 \pm 4.99$  h) and AD patients ( $n = 2$  females & 4 males; age =  $85.83 \pm 11.63$  years, PMD =  $8.5 \pm 7.45$  h; Braak & Braak stage IV) were obtained with ethical approval from the ethics committee of the University Medical Center Göttingen and upon informed consent from the Massachusetts Alzheimer Disease Research Center (NIA P50 AG05134, Boston, USA). *NEUID* expression data in human dorsolateral prefrontal cortex autopsy samples of the FHS participants are derived from previous publications [25].

The same human left ventricular heart tissue (RNA was already extracted) as previously described were used [26]. The samples represent healthy human hearts unassigned for transplantation. All performed experiments conform to the Declaration of Helsinki and all patients provided written informed consent for the use of cardiac tissue samples.

### 2.2 | Animals

The protocol to generate primary neurons and to collect tissue from adult mice was approved by the Lower Saxony State Office for Consumer Protection and Food Safety. C57B/6J or CD1 mice (Janvier Labs, Le Genest St Isle, France) were kept under a 12 h/12 h light/dark cycle, in standard single cages with food and water provided ad libitum. For obtaining brain subregions, liver and heart (left ventricle) samples for nuclei extraction or direct RNA extraction, adult animals were sacrificed via cervical dislocation and the organs were immediately removed on ice, followed by liver, left ventricle and anterior cingulate cortex (ACC) dissection. Other selected brain subregions (cortex, as well as dentate gyrus, CA1 and CA3 regions of hippocampus) were dissected in ice-cold PBS under a dissection microscope. Acquired tissue was snap-frozen in liquid nitrogen and stored at  $-80^{\circ}\text{C}$  until further processing. Behavioral experiment and stereotactic injection were approached by the animal care committee of the Albert Einstein College of Medicine, Bronx, NY, USA.

#### 2.2.1 | Stereotactic Surgery and Injection for Behavioral Experiments

Double-guided cannulas were implanted in the dorsal hippocampus (DH) as described previously. Mice were anesthetized with 1.2% tribromoethanol (vol/vol, Avertin) and implanted with bilateral 26-gauge cannulas using a stereotaxic apparatus. Stereotaxic coordinates for the dorsal hippocampus were 1.8 mm posterior,  $\pm 1.0$  mm lateral, and 2.5 mm ventral to bregma according to the mouse brain atlas (ventral coordinate updated from 2.0 mm to 2.5 mm). The *Neuid* and control (scrambled) Gapmers were

stored as 400 pmol/μl stock solutions at −80°C. Prior to use, Gapmers were heated to 65°C for 10 min, cooled on ice, and diluted 1:10 in artificial cerebrospinal fluid (aCSF) to a final concentration of 40 pmol/μl (buffer and concentration clarified). Seventy-two hours after cannula implantation, Gapmers were bilaterally injected into the dorsal hippocampus at a volume of 0.5 μl per hippocampus (20 pmol/site; 40 pmol/mouse) using an internal injector. For behavioral experiments, mice underwent either the open field test or contextual and trace fear conditioning 72 h after Gapmer injection. For molecular analyses, Gapmers were injected as described above, after which the hippocampus was dissected and immediately frozen in liquid nitrogen at the indicated time points (i.e., 48, 96 h after injection). Frozen tissue was stored at −80°C until RNA isolation and subsequent qPCR analysis.

### 2.3 | Fear Conditioning

Contextual fear conditioning was performed in an automated system (TSE Systems) as previously described [27]. Briefly, scramble ( $n = 4$  females & 5 males, age = 3 months) and *Neuid* ( $n = 6$  females & 2 males, age =) gapmer treated mice were exposed for 3 min to a novel context (A), followed by footshock (2 s, 0.7 mA, constant current) and tested 24 h later by re-exposing them to the same context. For trace fear conditioning, mice were exposed for 3 min to Context A followed by 3 consecutive pairings of tone (30 s, 75 dB, 10 kHz), temporal trace (15 s), and footshock (2 s, 0.7 mA, constant current). Memory tests were performed the next day by re-exposing the mice to Context B (3 min) followed by three presentations of tone (30 sec) and trace (15 s) separated by 60-s inter-trial intervals (ITI). Freezing, measured every 10 s, served as an index of memory. Freezing was expressed as a percentage of the total number of observations during which the mice were motionless. Activity was recorded automatically by an infrared beam system and expressed as cm/s. The individual experiments were not performed on littermates, so we did not apply randomization procedures, but all behavioral tests were performed by experimentalists who were unaware of the treatments because all injection solutions were coded by the lab technician.

### 2.4 | Nuclei Isolation

The isolation of nuclei from mouse and human brain tissue was performed according to our previous publications [28, 29] with minor modifications. Briefly, the tissue was homogenized using a dounce homogenizer in 500 μl EZ prep lysis buffer (Sigma NUC101) with 30 strokes (mouse tissue) or 60 strokes (Human tissue). The homogenate was transferred to 2 mL Eppendorf tube and the volume was adjusted to 2 mL with lysis buffer followed by 7 min incubation on ice. The homogenate was centrifuged for 5 min at 500 g at 4°C and the supernatant was discarded. The nuclei pellet was resuspended in 2 mL lysis buffer and incubated on ice for 5 min. The homogenate was centrifuged for 5 min (500 g at 4°C) and the pellet was resuspended in 1.5 mL nuclei storage buffer (NSB: 1 x PBS, 0.5% BSA, 1:200 RNase inhibitor, 1:100 Roche protease inhibitor) followed by another centrifugation for 5 min (500 g at 4°C). The obtained pellet was resuspended in 1 mL NSB and stained with anti-NeuN-AlexaFlour (Merck, MAB377X)

for 1 h at 4°C followed by centrifugation for 5 min (500 g at 4°C). The pellet was washed once with 500 μl NSB and resuspended in 300–500 μl NSB depending on the size of the pellet and stained with 1:100 7AAD (Invitrogen, Cat: 00–6993-50).

The samples were passed through a 40 μm filter into FACS tubes and vortexed before sorting. Sorting of NeuN-positive and NeuN-negative nuclei was performed with FACS Aria III (BD Biosciences). Sorted nuclei were counted in the Countess II FL Automated counter. The sorted nuclei were then used for Single-nuclei RNA-seq or centrifuged and resuspended in TRIzol-Is for RNA isolation.

### 2.5 | Single Nuclei Total RNA Sequencing and Analysis

Single-nuclei RNA-seq was performed at the NGS Integrative Genomics Core Unit in Göttingen, Germany. Approximately 1200 single cells were sequenced per sample. Single nuclei total RNA-seq was performed as described in Schröder et al., [30]. In short, nuclei were first stained with Hoechst 33342 that enables selection of suitable nuclei for dispensing into the Takara ICELL8 5184 nano-well chip. CellSelect Software (Takara Bio) was used to visualize and select wells containing single nuclei. Four 5184 non-well chips were used for samples containing 1200–1400 nuclei/sample. Libraries were amplified and pooled as they were extracted from each of the single nanowell chip. Purification and size selection of libraries was done with Agencourt AMPure XP magnetic beads (Beckman Coulter) to obtain an average library size of 500 bp. Libraries were sequenced on the HiSeq 4000 (Illumina) to obtain 0.3–0.4 Mio reads per nuclei (SE; 50 bp). Bcl2fastq (v2.20.2) was used for converting BCL files to FASTQ format from raw images. Further processing was performed with the Cogent NGS Analysis pipeline (v1.5.1) to generate a gene-count matrix. The demuxer (cogent demux) was used to create demultiplexed FASTQ files from the barcode sequencing data. The resulting output was then used as input for the analyzer (cogent analyze) which performs trimming, mapping, and gene counting to create a gene count matrix. Quality control was done by evaluating the quality report provided by the Cogent analyzer.

The SCANPY package was used for pre-filtering, normalization and clustering. First, cells with low quality were excluded. Then counts were scaled by total library size and transformed to log space. Highly variable genes were identified based on dispersion and mean, the technical influence of the total number of counts was regressed out, and the values were rescaled. Principal component analysis (PCA) was performed on the variable genes, and UMAP was run on the top 50 principal components (PCs). The top 50 PCs were used to build a k-nearest-neighbours cell-cell graph with  $k = 50$  neighbours. Subsequently, spectral decomposition over the graph was performed with 50 components, and the Leiden graph-clustering algorithm was applied to identify cell clusters. We confirmed that the number of PCs captures almost all the variance of the data. For each cluster, we assigned a cell-type label using manual evaluation of gene expression for sets of known marker genes by plotting marker gene expression on the UMAP and visual inspection. Violin plots for marker genes were created using the 'stacked\_violin function' as implemented in SCANPY.

## 2.6 | Primary Hippocampal Neuronal Culture

Primary hippocampal neuron cultures were prepared from CD1 mouse embryonic day 17 (E17) embryos representing mixed sex litters. Briefly, a pregnant CD1 mouse was sacrificed using pentobarbital and the brains of the embryos were isolated, meninges were removed, and the hippocampi were dissected. To obtain single-cell suspension the tissue was digested with 2.5% trypsin followed by DNase treatment. Cells were plated at a density of 60 000 cells/cm<sup>2</sup> in poly D-lysine coated multi-well plates and grown in Maintenance media (Neurobasal with 1xB27 and 1 mM GlutaMax). Primary hippocampal neurons were used for experiments at DIV10-21.

## 2.7 | Antisense LNA Gappers

Knockdown of *Neuid* in primary hippocampal neurons was performed by using Antisense LNA gappers packaged into Lipid nanoparticles (LNPs). The *Neuid* targeting and negative control (NC) gapmer was designed and purchased from Qiagen using the GeneGlobe Antisense LNA GapmeR Custom Builder, which selects RNase H-dependent GapmeRs without predicted RISC-associated off-target activity.

The following sequences were used:

NeuID: ACGAAAGCTTTTAACG

Nc: Gctcccttcaatccaa

To further assess GapmeR specificity, the antisense sequence was aligned against the full mouse transcriptome using BLAST to identify potential reverse-complement matches. This analysis identified *Neuid* as the only transcript with full sequence complementarity. The gappers were packaged into LNPs using the Neuro9 siRNA Spark Kit (5 nmol) with NanoAssemblr Spark system (Precision Nanosystems, Canada) according to the manufacturers instructions. Primary hippocampal neurons were transfected with *Neuid* targeting or NC LNPs on DIV 7 and the experiments were performed between DIV10-21.

## 2.8 | *Neuid* Overexpression with CRISPRa

Primary hippocampal neurons were transfected with AAV-PHP.eB serotype for *Neuid* overexpression (OE). AAV vectors containing the guide RNA (gRNA) plasmid and the dCas9-VP64 expression plasmid were purchased from Vectorbuilder. The *Neuid* targeting gRNA and scrambled negative control had the following sequences:

gRNA – 1 : GCGCCGGCTTGATTCCCGGTG

gRNA – 2 : CGCGAGCCCGGGAGGACGCGG

Nc: Gtgtagctgaccattcgtg

Primary hippocampal neurons were co-transfected with the gRNA containing AAVs and the dCas9-VP64 expressing AAVs at different multiplicity of infection (MOI) at DIV 7 to determine the optimum MOI. For NeuID OE experiments, primary hippocampal

neurons were co-transfected with dCas9-VP64 expressing AAV and scramble or *Neuid* targeting gRNA containing AAV at DIV 7. For all OE experiments, transfection was performed at DIV7 and experiments were performed 48 h later.

## 2.9 | Treatment of Primary Hippocampal Neurons

A $\beta$ 1-42(Cayman chemicals) was prepared as previously described in Schröder et al., [30]. Briefly, A $\beta$ 1-42 was incubated at 37°C for 1 h and added to primary hippocampal neurons at a concentration of 1  $\mu$ M for 24 h.

To assess *Neuid* expression upon exposure to different neuronal stimulants or inhibitors, primary hippocampal neurons were treated with Bicuculline (Sigma-Aldrich), Muscimol (Sigma-Aldrich), and Tetrodotoxin (Tocris) at a concentration of 1  $\mu$ M for 24 h.

## 2.10 | RNAscope

RNAscope fluorescent multiplex assay (ACD Bio) combined with immunofluorescence for fresh frozen tissue sections was performed according to the manufacturer's instructions and as described in Schröder et al., [30]. Briefly, sections were fixed in 10% neutral buffered formalin (NBF), dehydrated with ethanol, and treated with hydrogen peroxide followed by ON incubation at 4°C with anti-NeuN (abcam, ab177487). The following day, in accordance with the RNAscope Multiplex Fluorescent Reagent Kit v2 (ACD Bio) protocol, probes designed against NeuID (ACD Bio) and TSA Plus Cyanine 5 (Akoya Biosciences, 1:1750) for detection were used. Afterwards, the sections were stained with Alexa Flour 555 goat anti-rabbit secondary antibody (1:1000, ThermoFischer) and DAPI (Sigma-Aldrich). Images were acquired within a week after staining. RNAscope signal intensity was quantified using FIJI (ImageJ). Equivalent regions of interest (ROIs) were selected for each image and added to the ROI Manager. Signal intensity for each ROI was obtained using the Measure function in FIJI. To normalize for ROI size, the measured signal intensity was divided by the ROI area, yielding signal intensity per unit area.

## 2.11 | Dendritic Spine Labelling

Dendritic spine density analysis on primary hippocampal neurons was performed as described previously [30]. The cells were fixed with 2% paraformaldehyde (PFA) and washed 3x with PBS. For staining, 2–3 crystals of the DiI stain (Life technologies-Molecular Probes) were added to each well and incubated on a shaker for 10 min at RT. The cells were then washed until there were no visible DiI crystals in each well and incubated overnight at RT in PBS. Images were taken 72 h later. Dendritic spine density was measured using the dendritic spine counter plugin in ImageJ software.

## 2.12 | Synapse Quantification

Synapse density quantification was performed by using a dual-color staining of pre- and post-synaptic markers along with

staining of the neuronal body. The cells were fixed with PFA (4%, 10 min, RT) and permeabilized with 1% Triton X-100 in PBS followed by incubation in blocking buffer (2% BSA in PBS) for 1 h at RT. The cells were then incubated with primary antibodies—Synaptophysin (Synaptic Systems, 101 008), Psd95 (Synaptic Systems, 124 011), Map2 (Synaptic Systems, 188 006) in a blocking buffer overnight at 4°C. After washing with PBS, the cells were incubated with Alexa Fluor 633 goat anti-rabbit (ThermoFisher Scientific, A21071), Alexa Fluor 555 goat anti-mouse (ThermoFisher Scientific, A21424), and Alexa Fluor 488 goat anti-chicken (abcam, ab150169) secondary antibodies in blocking buffer for 1 h at RT. Synapse density was calculated using synquantvid plugin in ImageJ software.

### 2.13 | Multielectrode Array Recording and Data Analysis

To record spontaneous activity from primary hippocampal neurons, the Maestro Edge multiwell microelectrode array (MEA) system (Axion Biosystems) was used. The Cytoview MEA 24, with 24 wells and 16 electrodes per well was used for the recordings. Primary hippocampal neuron culture was performed as described in a previous section, and the cell pellet was suspended in Maintenance Media with 1 µg/ml laminin to a concentration of 12.5 x 10<sup>6</sup> neurons/ml. 8 µl of the cell suspension was added to each well of the MEA plate pre-coated with polyethylenimine. For recording, the MEA plate containing neurons was transferred to the recording chamber maintained at 37°C with 5% CO<sub>2</sub>, and the activity was recorded for 15 min. Data from the MEA was analyzed using the manufacturer's analysis tool 'Neural Metric Tool (Axion Biosystems)'. A spike was computed with an adaptive threshold of six standard deviations of the estimated noise for each electrode. Bursts were identified using an inter-spike interval (ISI) threshold of a minimum five spikes within an ISI of 100 ms. Network bursts represent co-ordinated bursts across multiple electrodes and were calculated as bursts of minimum 50 spikes within an ISI of 100 ms that occurred across more than 35% of the active electrodes. Synchrony represents simultaneous spiking between electrodes and the synchrony index was estimated by the area under the normalized cross-correlogram for a time window of 20 ms.

### 2.14 | Imaging

All images were taken with the STEDycon STED/Confocal (Abberior) in the confocal mode at 63X oil immersion objective.

### 2.15 | Nuclear and Cytoplasmic Fractionation for qPCR Analysis

Nuclear and cytoplasmic fractions were obtained using the Nuclei EZ PREP Nuclei isolation kit (NUC-101, Sigma) based on manufacturer's instruction with minor modifications. Briefly, 500 µl ice cold Nuclei EZ lysis buffer supplemented with RNase inhibitor (Promega) was added to each well and the cells were scraped and collected. The cells were then incubated on ice for 7 min. The samples were then centrifuged at 500 g for 5 min. at 4°C and the supernatant was aspirated and collected,

containing the cytoplasmic fraction. The nuclear pellet was washed with 2 mL EZ prep lysis buffer, incubated on ice and centrifuged again. The pellet was resuspended in 1.5 mL nuclei storage buffer (NSB: 1 x PBS, 0.5% BSA, 1:200 RNase inhibitor, 1:100 Roche protease inhibitor) and centrifuged again. TrizolLS Reagent (ThermoFisher) was added to both the cytoplasmic and nuclear fraction and the samples were stored at -20°C until RNA isolation was performed.

### 2.16 | RNA Isolation, cDNA Synthesis and RT-qPCR

Total RNA was isolated from cells or tissues using TRIzol (Invitrogen) and purified with RNA clean & concentrator-5 (Zymo research) according to the manufacturer's instructions. RNA concentration was measured with nanodrop (ThermoFischer). Total RNA was reverse transcribed into cDNA using transcription first strand cDNA synthesis kit (Roche). RT-qPCR was performed on LightCycler 480 system (Roche) using the SYBR Green I Master (Roche) with primers listed in supplemental table 10 The data was analyzed using the 2-ddCt method.

### 2.17 | RNA-seq and Analysis

RNA quality was determined using Bioanalyzer (Agilent) prior to library preparation. Library preparation for RNA-seq was performed using SMARTer Stranded Total RNA-seq kit v2-pico input according to the manufacturer's instructions. Five ng of total RNA was used as input for library preparation. The quality and size of the library was determined using Bioanalyzer. The multiplexed libraries were sequenced in a HiSeq 2000 (Illumina) with a 50 bp single-read configuration.

The sequencing data was processed using a customized in-house software pipeline. Illumina's conversion software bcl2fastq (v2.20.2) was employed for adapter trimming and converting the base calls in the per-cycle BCL files to the per-read FASTQ format from raw images. Quality control of raw sequencing data was carried out using FastQC (v0.11.5) (<http://www.bioinformatics.babraham.ac.uk/projects/fastqc/>). Reads were aligned using the STAR aligner (v2.5.2b) and read counts were generated using featureCounts (v1.5.1). The mouse genome version mm10 was utilized. Differential gene expression analysis was performed with DESeq2 (Version 1.42) [31] with RUVseq to correct for unwanted variation. GO term analysis was performed with ClueGO plugin in Cytoscape. Analysis for the enrichment of transcription factors was performed using ENRICH (https://maayanlab.cloud/Enrichr/).

### 2.18 | Promoter Region Analysis

The promoter regions for 892 genes upregulated after loss of *Neu1D* were obtained from the Ensembl database using Mus musculus genome GRCm39. Promoter regions were defined as 1000 bp before TSS. The sequences were extracted using SAMtools (v1.10). Binding motifs for the glia-specific transcription factors were taken from the JASPAR (v2022) database. We used

BLAMM (v1.0.0) to screen promoter regions for TF binding motifs.

## 2.19 | RNA Immunoprecipitation

The nuclear fraction was obtained from cultured primary hippocampal neurons using Nuclei isolation kit (Sigma, NUC101) according to manufacturer's instructions. The obtained nuclear fraction is resuspended in TSE buffer (10 mM Tris, 300 mM sucrose, 1 M EDTA, 0.1% Nonidet P-40, 100 units/ml RNase inhibitor, 1x protease inhibitor), transferred to bioruptor tubes (Diagenode) and sonicated in a Bioruptor Plus (Diagenode) for 5 cycles (30s on, 30s off). The samples were then incubated on ice for 20 min with occasional vortexing and centrifuged for 10 min at 13000 rpm at 4°C. The supernatant was transferred to a fresh tube and flash frozen at -80°C. The lysate was precleared using 25 µl Pierce Protein A/G magnetic beads (ThermoFischer) for 1 h at 4°C to reduce unspecific binding. Anti-EZH2 (Millipore) or IgG isotype control (Millipore) was incubated with 50 µl Protein A/G magnetic beads for 2 h at RT and washed with RNA-IP buffer (50 mM Tris-HCl, 100 mM NaCl, 32 mM NaF, 0.5% NP-40). 10 % of the lysate was kept as input and the beads were added to the remaining lysate and incubated overnight at 4°C on a rotator. Then the beads were washed 5x with RNA-IP buffer, and incubated in proteinase K in proteinase K buffer (Qiagen) for 1 h at 37°C. The supernatant was collected and RNA extracted using the RNA clean & concentrator-5 kit (Zymo research) according to manufacturer's instructions. Total RNA was reverse transcribed into cDNA using transcription first strand cDNA synthesis kit (Roche). RT-qPCR was performed on LightCycler 480 system (Roche) using the SYBR Green I Master (Roche) to quantify amounts of *NeuID* transcripts present in the Anti-EZH2 and IgG isotype control immunoprecipitated (IP) lysates. *NeuID* binding to EZH2 or IgG control was analyzed with the % input method, where *NeuID* in IP-fraction is quantified as a percentage of *NeuID* present in the input fraction. Briefly, to calculate the % input, qPCR was performed for *NeuID* on the input, anti-EZH2, and IgG isotype control fractions. Because only a small fraction of the lysate was set aside as the input sample, the qPCR value for *NeuID* in the input is mathematically adjusted to represent the amount present in the entire starting lysate. *NeuID* levels in the anti-EZH2 and IgG IP fractions are then expressed as a percentage of this normalized input value. The resulting % input reflects the proportion of total *NeuID* RNA that is bound to EZH2 or recovered in the IgG isotype control

## 2.20 | Chromatin Immunoprecipitation

Primary hippocampal neurons were cultured in 6-well plates and treated with control or *NeuID* targeting LNPs as described above. To each well 1 mL of Low sucrose buffer (0.32 M sucrose, 5 mM CaCl<sub>2</sub>, 5 mM Mg(Ac)<sub>2</sub>, 0.1 mM EDTA, 10 mM HEPES, 0.1 % Triton X-100, 1 mM DTT, 1x Protease inhibitor) was added and the cells were collected from each well using a cell-scraper and immediately flash frozen in liquid nitrogen. To prepare chromatin for ChIP, the cells were thawed and cross-linked using 5% PFA for 10 min. The reaction was quenched by adding 125 mM glycine for 5 min followed by centrifugation at 1000 g for 3 min at 4°C. The supernatant was discarded and the nuclei pellet was resuspended

in 500 µl Nelson buffer (140 mM NaCl, 20 mM EDTA, 50 mM Tris pH 8.0, 0.5% NP-40, 1 % Triton X-100, 1x protease inhibitor). The nuclei suspension was then homogenized using mechanical homogenizer (Ultraturax T10) with power on 4 for 10s. The suspension was then centrifuged at 10 000 g for 2 min at 4°C, and the pellet was washed once with Nelson buffer. Afterwards, the supernatant was discarded and the nuclei pellet was weighed and resuspended in 10x volume of RIPA buffer (140 mM NaCl, 1 mM EDTA, 1 % Triton X-100, 0.1% sodium deoxycholate, 10 mM Tris-Cl, 1 % SDS, 1x Protease inhibitor). The samples were then incubated at 4°C on a wheel for 10 min and then sonicated for 30 cycles (30s on, 30s off). To check chromatin shearing a small amount of chromatin was aliquoted and de-crosslinked by proteinase K treatment for 1 h at 65°C. DNA was isolated using Zymo ChIP clean and concentrator kit (Zymo research) according to manufacturer's instructions. The size of the sheared chromatin was determined by using Bioanalyzer 2100 with a DNA high sensitivity kit and the concentration was measured using Qubit 2.0 fluorometer (DNA high sensitivity kit). 1 µg of chromatin and 3 µg of antibody was used for H3K27me3 (Millipore) or IgG isotype control (Millipore) chIp.

## 2.21 | ChIP Sequencing and Analysis

The ChIP DNA was used for library preparation using NEBNext Ultra II DNA library preparation kit (New England Biolabs). Libraries were sequenced for single end 50 base pair reads with the NextSeq 2000 (Illumina). Base calling and fastq conversion of sequencing data was performed using the Illumina pipeline and quality control was performed using fastqc (v0.11.5). Reads were mapped to mm10 mouse reference genome using bowtie2. MACS2 [32] was used for calling peaks with the option 'broad-peaks' and q value < 0.1. ngsplot was used to create profile plots. Diffbind package was used for differential binding analysis with in-built DESEQ2 option for differential analysis. ChIPSeeker package of Bioconductor was used for annotation of peaks.

## 2.22 | Statistical Analysis

Statistical analysis was done using GraphPad Prism version 9. All graphs are represented as mean ± SEM unless stated otherwise. A two-tailed unpaired t-test or one-way ANOVA was used for analysis unless otherwise stated.

## 2.23 | Datasets Used in this Study

The following snucRNAseq datasets were used in this study. The human snucRNAseq datasets were from Schröder et al. [30]. The snucRNAseq data from the mouse brain are from.

## 3 | Results

### 3.1 | *NeuID* Is a Conserved lncRNA Highly Enriched in Neurons of the Adult Brain

The primary objective of this study was to identify neuron-specific long non-coding RNAs (lncRNAs) that are enriched

in brain tissue compared to other organs and to investigate their roles in Alzheimer's disease (AD). We hypothesized that identifying such lncRNAs could reveal promising drug targets with minimal off-target effects, given their brain- and cell-type-specific expression. To test this, we integrated publicly available datasets with cell-type-specific total RNA sequencing (RNA-seq) and single-nucleus RNA sequencing (snRNA-seq) data from mouse and human brains (Figure 1a). The inclusion of both species was based on the premise that, particularly for lncRNAs, cross-species conservation is an indicator of functional relevance [5, 30].

We began our analysis with mouse tissue by performing fluorescence-activated nuclear sorting (FANS) on the hippocampal CA1 region, a brain area essential for memory formation and among the first affected in AD. We isolated neuronal (NeuN<sup>+</sup>) and non-neuronal (NeuN<sup>-</sup>) nuclei from three-month-old wild-type mice (Figure S1) and performed total RNA sequencing (Figure 1a, box 1). This analysis identified 247 lncRNAs that were significantly enriched in NeuN<sup>+</sup> compared to NeuN<sup>-</sup> nuclei ( $p < 0.05$ ,  $\log_2 FC > 3$ ; Table S1).

Next, we investigated whether any of these lncRNAs had human homologs (Figure 1a, box 2). We identified homologous lncRNAs based on shared syntenic genomic loci and a minimum sequence similarity of 40% [30, 33]. Using this approach, we identified 15 candidate lncRNAs (Table S2). To further refine this selection, we leveraged a human RNA tissue atlas [30, 34] and the GTEx database (<https://gtexportal.org>) to filter for brain-enriched expression patterns (Figure 1a, box 3; Figure S2). This led us to a lncRNA, previously unstudied, referred to as *ENSG00000283183* in humans and *Gm10419* in mice, which showed the highest enrichment in the human brain compared to other tissues (Figure 1b–d; Figure S2). Outside the brain, expression of *ENSG00000283183* was detected only in the pituitary, for which data were available in the GTEx database but not in the RNA Atlas. Moreover, the GTEx portal suggests relevant levels of *ENSG00000283183* expression in skin, whereas the RNA Atlas reports very low to non-detectable expression in the dermal system. Given our later findings, we named this lncRNA *Neuronal Identity (NEUID)*. In the following, *Neuid* refers to the mouse transcript, and *NEUID* to its human homologue.

To further validate the neuronal and brain-specific expression of *Neuid*, we performed qPCR analysis on NeuN<sup>+</sup> and NeuN<sup>-</sup> nuclei isolated from the mouse hippocampal CA1 region. Consistent with our sequencing data, qPCR confirmed that *Neuid* was exclusively expressed in NeuN<sup>+</sup> nuclei (Figure 1e). Additionally, single-nucleus RNA sequencing (snRNA-seq) of mouse brain tissue confirmed that *Neuid* is highly enriched in neurons compared to glial cells (Figure 1f).

To determine whether a similar expression pattern exists in the human brain, we performed FANS on NeuN<sup>+</sup> and NeuN<sup>-</sup> nuclei isolated from the prefrontal cortex of individuals without neurodegenerative disorders (Figure S1). qPCR analysis revealed that *NEUID* was highly enriched in NeuN<sup>+</sup> nuclei, mirroring our findings in mice (Figure 1g). Furthermore, snRNA-seq analysis of the human prefrontal cortex confirmed that *NEUID* is significantly enriched in neurons compared to glial cells (Figure 1h). Please note that expression levels from the mouse and human

snucRNA-seq datasets should not be compared directly, as the mouse data were generated using the 10x Genomics platform [29], whereas the human data were obtained using a modified Takara iCELL8-based protocol optimized for improved lncRNA detection [30].

Finally, we further validated these findings in bulk tissue by performing qPCR analysis on total RNA isolated from the human prefrontal cortex and heart (left ventricle). The heart was chosen since, next to the brain, it is the only other organ that mainly consists of postmitotic and excitable cells. *NEUID* expression was significantly higher in the brain, with negligible expression detected in the heart (Figure 1i).

We also assessed *Neuid* expression across different mouse brain regions using qPCR and compared it to expression levels in the heart and liver. *Neuid* was consistently highly expressed in all analyzed brain regions, with minimal or undetectable expression in the heart and liver (Figure 1j).

In summary, we identified *NEUID* as a previously uncharacterized lncRNA with a neuron-specific and brain-enriched expression pattern in both mice and humans. Next we wanted to test if *NEUID* is deregulated in neurodegenerative diseases (Figure 1a, Box 4).

### 3.2 | NEUID is Down-Regulated in the Brains of AD Patients

Given the emerging role of ncRNAs as novel drug targets in neurodegenerative diseases, we investigated whether *NEUID* is dysregulated in the brains of AD patients. Analysis of data from the AGORA database, which includes over 1000 brain samples from healthy individuals and AD patients, revealed that *NEUID* expression is significantly reduced in the parahippocampal gyrus (PHG), dorsolateral prefrontal cortex (DLPFC), and temporal cortex (TCX) of AD patients compared to controls (Figure 2a).

To confirm this observation, we performed qPCR analysis on a smaller cohort of postmortem brain samples characterized by Braak & Braak (B&B) stage IV. B&B staging is a widely used classification system for assessing the severity of AD pathology. B&B stages range from stage 1, representing minimal neurofibrillary tangle deposition, to stage 6, which indicates advanced, widespread pathology [35]. In agreement with the AGORA findings, *NEUID* expression was significantly decreased in the prefrontal cortex (B&B stage IV, representing an early to moderate disease stage in the prefrontal cortex) when compared to controls (Figure 2b).

We further analyzed *NEUID* expression using the previously-described RNASeq dataset from brain tissue (prefrontal cortex, area 9) from the Framingham Heart Study [36, 25], focusing on samples spanning all B&B stages. Consistent with our prior results, *NEUID* expression was negatively correlated with B&B stages ( $r = 0,31$ ;  $p = 0,049$ ), indicating a progressive decline as pathology worsens (Figure 2c).

It is important to note that *NEUID* expression varies substantially among individuals, which is not unexpected in analyses of

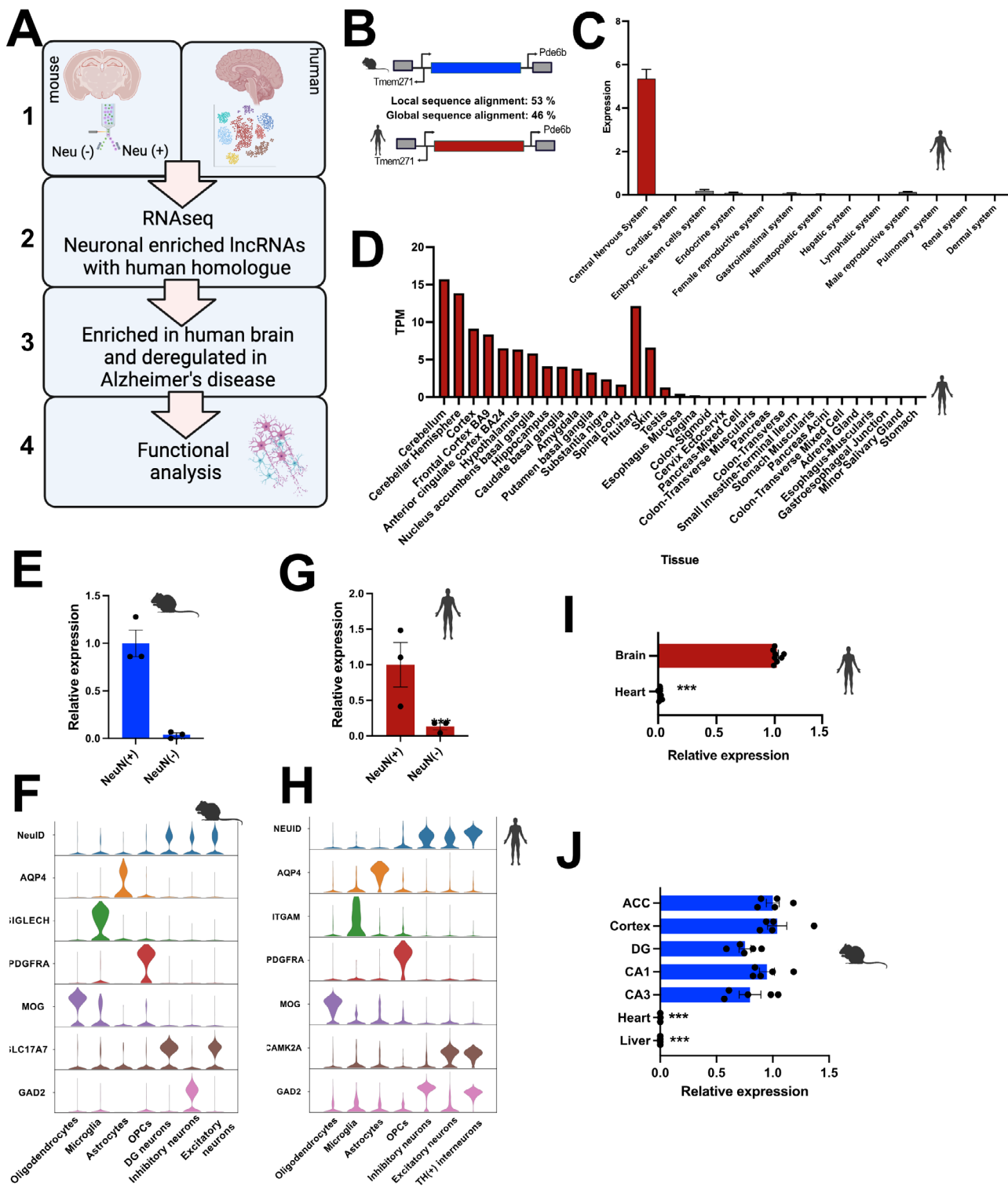


**FIGURE 1** | *NEUID* is a conserved lncRNA highly enriched in neurons of the adult brain. (A) Schematic overview of the experimental approach. (B) Schematic illustration showing the genomic localization of mouse *NeuID* and human *NEUID*. (C) Expression of *NEUID* across various human tissues obtained from the RNA-atlas (Expression is quantified as read counts per million), and (D) the GTEx tissue expression database (<https://gtexportal.org>). TPM: Transcripts per million. (E) Bar chart showing qPCR analyses of *NeuID* expression between NeuN(+) ( $n = 3$ ) and NeuN(-) ( $n = 3$ ) nuclei obtained from the hippocampal CA1 region of mice. (F) Violin plot depicting the expression of *NeuID* in a snucRNA-seq dataset from mice brain along with marker genes for the depicted cell types. (G) Bar chart showing qPCR analyses of *NEUID* expression in NeuN(+) ( $n = 3$ ) and NeuN(-) ( $n = 3$ ) nuclei from the human prefrontal cortex. (H) Violin plot depicting the expression of *NEUID* in a snucRNA-seq dataset obtained from the human prefrontal cortex along with marker gene expression or the depicted cell types. (I) Bar chart showing qPCR analyses of *NEUID* expression in human brain (prefrontal cortex,  $n = 8$ ) and heart tissue (left ventricle,  $n = 9$ ). (J) Bar chart showing qPCR analyses of *NEUID* expression in different mice brain areas ( $n = 5$ ), heart ( $n = 3$ ) and liver ( $n = 4$ ). ACC: Anterior cingulate cortex, DG: Dentate Gyrus, CA1/3: Cornu Ammonis 1/3. Asterisk indicates statistical significance analyzed via unpaired tTest. \*\*\* $p < 0.0001$ . Error bars indicate SEM.

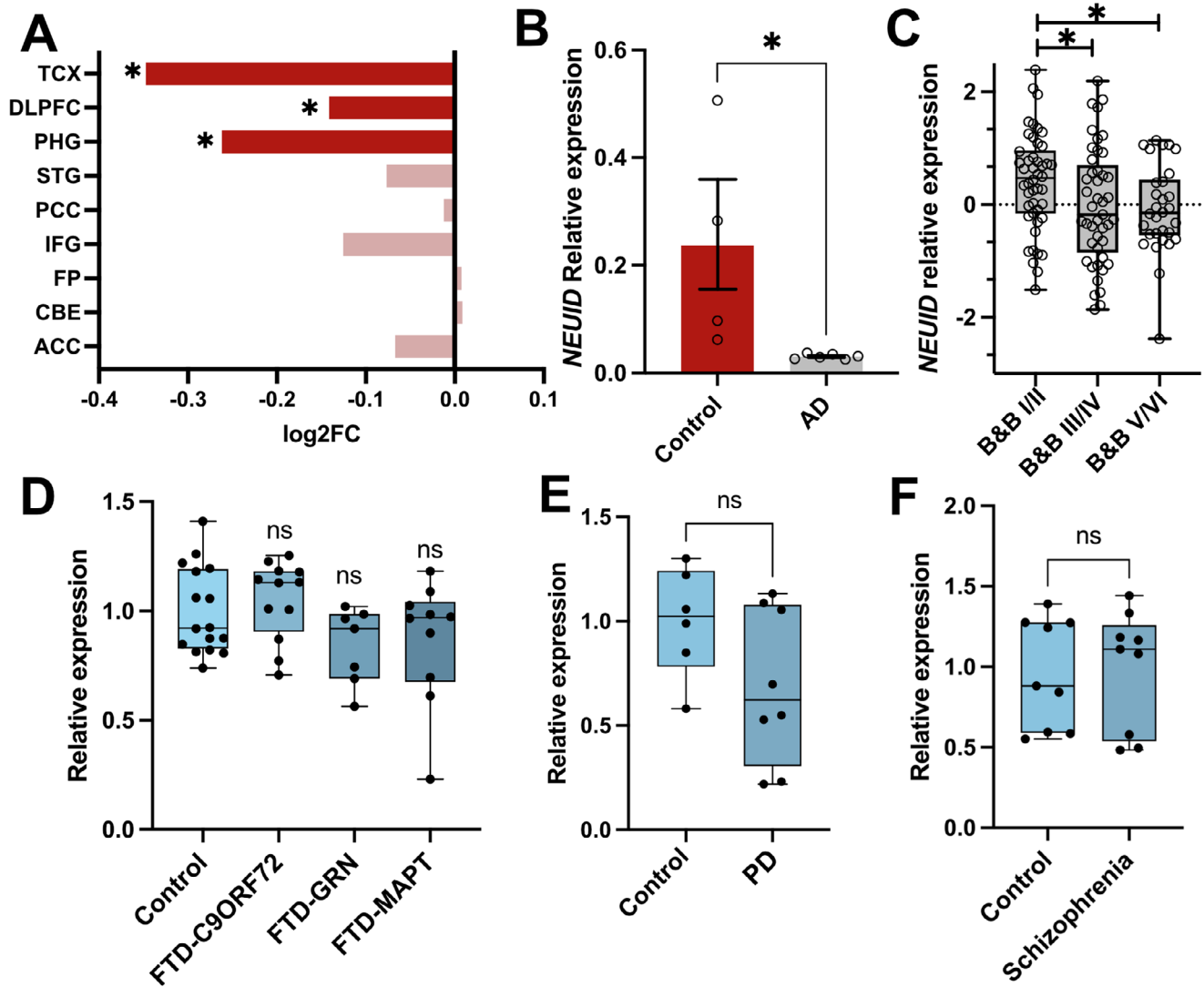


**FIGURE 2** | *NEUID* is down-regulated in the brains of AD patients. (A) *NEUID* expression in various brain regions of AD and control postmortem human brains. Data were obtained from the AGORA AD database ( $*p < 0.05$ ). (B) qPCR analysis of *NEUID* expression in prefrontal cortex (Brodmann Area 9, BA9) postmortem brain tissue from control ( $n = 4$ ) and AD ( $n = 6$ ) patients (Unpaired tTest;  $*p < 0.05$ ). (C) Expression of *NEUID* in postmortem brain tissue from individuals spanning Braak & Braak (B&B) stages I–VI. Data were obtained from the Framingham Heart Study (One way ANOVA;  $p = 0.034$ ). A two-way ANOVA including diagnosis and sex revealed a significant main effect of diagnosis ( $p = 0.0429$ ), but no main effect of sex or diagnosis $\times$ sex interaction. (D) Box plot showing *NEUID* expression in the frontal cortex of FTLD patients with mutations in C9ORF72 ( $n = 12$ ), GRN ( $n = 7$ ), MAPT ( $n = 10$ ), and controls ( $n = 16$ ) ( $ns = \text{not significant}$ ). (E) Box plot of *NEUID* expression in the frontal cortex of Parkinson's disease (PD) patients ( $n = 8$ ) and controls ( $n = 6$ ). Data were obtained from the GEO dataset GSE156928 ( $ns = \text{not significant}$ ). (F) qPCR analysis of *NEUID* expression in the prefrontal cortex (BA9) of schizophrenia patients ( $n = 9$ ) and controls ( $n = 9$ ) ( $ns = \text{not significant}$ ). Abbreviations: TCX, temporal cortex; DLPFC, dorsolateral prefrontal cortex; PHG, parahippocampal gyrus; STG, superior temporal gyrus; PCC, posterior cingulate cortex; IFG, inferior frontal gyrus; FP, frontal pole; CBE, cerebellum; ACC, anterior cingulate cortex; FTD, frontotemporal dementia; PD, Parkinson's disease.

postmortem human tissue and is likely attributable to factors that, at present, cannot be controlled for, such as environmental factors, medication or inter-individual genetic background.

Interestingly, no significant changes in *NEUID* expression were detected in RNA-seq datasets derived from postmortem brain tissue of patients with frontotemporal lobar degeneration (FTLD) [37, 38] (Figure 2d), Parkinson's disease (PD) (GEO dataset GSE156928) (Figure 2e), or schizophrenia [39] (Figure 2f). This indicates that *NEUID* dysregulation may be primarily associated with AD pathology and moreover suggest that decreased *NEUID* levels are not simply a result of neuronal cell death. To further

address this issue, we analyzed the expression of the neuronal marker gene *RBFOX3* (*NEUN*), which can serve as a proxy for neurodegeneration when tissue for immunohistochemical analysis is not available [40]. Within the AGORA dataset, there was no significant correlation between *NEUID* and *RBFOX3* changes across all analyzed tissues (Pearson's  $R^2 = 0.008$ ;  $p = 0.82$ ). Moreover, unlike *NEUID*, *RBFOX3* was not significantly decreased in the TCX and DLPFC. However, its levels were reduced in the PHG (Figure S3), which is in agreement with findings showing that the PHG is affected much earlier during the course of AD pathogenesis compared to the TCX or DLPFC [41]. In line with this observation, *RBFOX3* levels were not altered

when we performed qPCR analysis of prefrontal cortex post-mortem tissue samples used in Figure 2b, or when we analyzed data from the FHS (Figure S3). Finally, It should be mentioned that there is a non-significant trend for decreased expression of *NEUID* in PD patients and that it would be interesting to analyze a larger dataset in future studies.

### 3.3 | Knock Down of NeuID Affects Neuronal Gene-expression

To the best of our knowledge, *Neuid* has not been studied in any cellular context. Given our data showing that *NEUID* is enriched in neurons, almost exclusively expressed in the brain, and decreased in the brains of AD patients, we sought to elucidate its function.

Since lncRNAs perform regulatory functions specific to their cellular localization [42], we first assessed the localization of *Neuid*. To this end, we performed RNAscope in adult mouse brain sections, combined with NEUN staining to label neuronal nuclei. Our data confirmed that *Neuid* is highly expressed in neurons and further suggested that *Neuid* is enriched in neuronal nuclei, as shown by the high proportion of *Neuid*-positive nuclei co-labeling with the neuronal marker NeuN (Figure 3A,B). Interestingly, two to ten bright foci of *Neuid* of different size were observed per neuronal nucleus, a pattern consistent with previous lncRNA studies and has been associated with the regulation of chromatin dynamics [43, 44]. Consistent with this observation, qPCR analysis revealed that *Neuid* is enriched in nuclear fractions isolated from the mouse hippocampus compared to cytoplasmic fractions (Figure 3C), further suggesting a potential role in gene expression regulation.

To investigate *Neuid*'s function, we performed *Neuid* knock-down (KD) in primary hippocampal neurons using Gapmers, single-stranded antisense oligonucleotides that mediate RNase H-dependent degradation of nuclear RNA transcripts. As a negative control, we used Gapmers with no known target in the genome.

First, we assessed the efficacy of *Neuid* knockdown by qPCR analysis at multiple time points (0.5, 1, 1.5, 2, 4, 6, 7, 25, and 72 h) after Gapmer administration. *Neuid* expression was fully suppressed 72 h post-treatment (Figure 3D) and still detectable when measured up to 16 days post-treatment (Figure S4). We decided to use the 72 h time point for RNA sequencing (RNA-seq) to determine the effects of *Neuid* KD on the hippocampal neuronal transcriptome. *Neuid* knockdown efficacy was confirmed by qPCR for the RNAseq experiment (Figure 3E). RNA-seq analysis revealed 892 upregulated and 597 downregulated genes following *Neuid* KD (false discovery rate [FDR];  $\text{padj} < 0.05$ ,  $\text{FC} > 0.5$  or  $< -0.5$ ; Figure 3F; Tables S3 and S4). Gene Ontology (GO) term analysis showed that upregulated genes were enriched in biological processes (Table S5) related to development and glia cell function including the GO terms such as “regulation of developmental processes”, “nervous system development”, “gliogenesis” and “glia cell differentiation” (Figure 3G). For the down-regulated genes we detected much less significant GO-terms, when compared to the up-regulated genes including the GO terms “signal transduction”, “gene expression” and “neuropeptide signaling

pathway” (Figure 3G; Table S6). These data indicate that *Neuid* loss drives a coordinated transcriptional shift toward glial and developmental gene programs, as reflected by enrichment of astrocyte- and oligodendrocyte-expressed genes among upregulated transcripts and neuronal genes among downregulated transcripts (Figure 3H).

To validate these RNA-seq findings, we confirmed the altered expression of selected genes using qPCR. Our data show increased expression of non-neuronal genes, including oligodendrocyte transcription factor 2 (*Olig2*), which is normally expressed in oligodendrocytes; S100 calcium-binding protein B (*S100B*) normally expressed in astrocytes and apolipoprotein E (*ApoE*), normally expressed in astrocytes and microglia (Figure 3I). Conversely, genes such as gamma-aminobutyric acid type A receptor subunit alpha-3 (*Gabra3*), regulator of G-protein signaling 4 (*Rgs4*), and 5-hydroxytryptamine receptor 5A (*Htr5a*), whose loss of function has been linked to cognitive impairments [45–47], were downregulated (Figure 3I). These data indicate that *Neuid* plays a role in the orchestration of neuron-specific gene expression, as its reduced levels lead to increased expression of non-neuronal genes linked to developmental glial-related processes. This is paralleled by the downregulation of neuronal genes linked to memory function.

### 3.4 | NeuID Regulates Neuronal Activity, Synapse Number and Memory Formation in Mice

The analysis of neuronal gene-expression upon *Neuid* KD suggests that *Neuid* may play an important role in the regulation of neuronal functions and the loss of *Neuid* expression, as observed in AD patients, may cause deregulation of neuronal plasticity. To address this directly we decided to study neuronal network plasticity upon *Neuid* KD. Therefore, primary hippocampal neurons were subjected to electrical recordings using multi-electrode arrays (MEA). Although *NEUID* downregulation in AD patients was assessed in cortical tissue, *Neuid* expression is highly comparable across hippocampal and cortical regions in adult mice (see Figure 1j and Figure 3a), indicating that its physiological expression is not region-restricted within the forebrain. Importantly, the hippocampus is among the earliest and most severely affected regions in AD [35, 48], and high-quality human hippocampal tissue from early disease stages was not available to us either through tissue banks or through large transcriptomic resources such as the AGORA database. Consequently, cortical tissue provides the most reliable window into *NEUID* deregulation in patients, whereas the hippocampus represents the most appropriate model system to mechanistically dissect how loss of *Neuid* affects neuronal plasticity. Therefore, hippocampal neurons were plated on MEA plates and *Neuid* KD was performed on DIV7. The MEA activity was recorded 72 h later at DIV10 for 15 min.

Loss of *Neuid* resulted in severe impairments of neuronal network activity as indicated by a reduced neural activity score (NAS), a composite score that serves as an objective metric to compare neuronal activity in MEA [49, 50] (Figure 4a) and a significantly decreased mean firing rate, which reflects the average number of action potentials detected per electrode per second and serves as an indicator of global neuronal excitability (Figure 4b). These

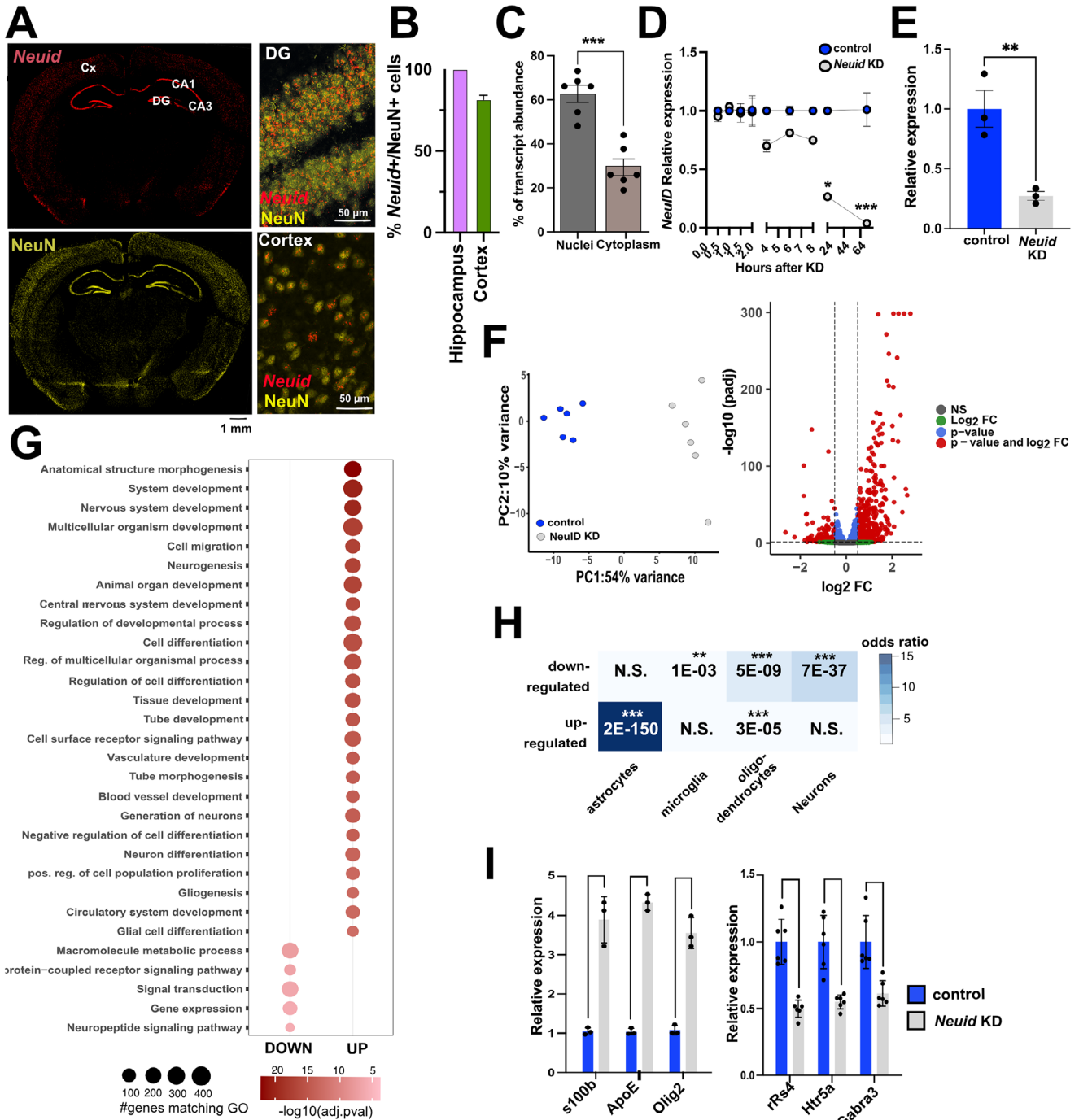


**FIGURE 3** | Knock down of *Neuid* affects neuronal gene-expression. (A) Representative images from the adult mouse brain (3 months old male C57Bl/6J mice) showing RNAscope signals for *Neuid* (red, upper left panel) and neuronal nuclei stained with NeuN (yellow, lower left panel). The right panel shows higher magnification images of the hippocampal DG region (upper right panel) and the cortex (lower right panel). (B) Bar chart showing the quantification of the number of *Neuid*-positive (*Neuid*<sup>+</sup>) and NeuN-positive (NeuN<sup>+</sup>) nuclei in the hippocampal and cortical regions. (C) RT-qPCR quantification of *Neuid* expression in nuclear and cytoplasmic fractions of hippocampal neurons ( $n=6$ ). unpaired tTest;  $***p < 0.001$ . (D) RT-qPCR quantification of NeuID expression at indicated time points following administration of *Neuid* Gapmers or control Gapmers in hippocampal neurons. One-way ANOVA revealed a significant group difference ( $p < 0.0001$ ,  $F = 16.91$ );  $*p < 0.05$ ,  $****p < 0.0001$ . (E) Bar plot showing *Neuid* knockdown in RNA-seq samples ( $n=3$ ).  $**p < 0.01$ , unpaired tTest. (F) Left panel: Principal component analysis (PCA) of the RNAseq data. Right panel: Volcano plot depicting differentially expressed genes following *Neuid* KD ( $FDR < 0.05$ ,  $|\log_2FC| > 0.5$ ). (G) Dot plot showing the top 10% Gene Ontology (GO) terms (biological processes) associated with upregulated and downregulated genes after *Neuid* KD. (H) Heatmap showing cell-type specific enrichment of the up- and downregulated genes.  $*p < 0.05$ ,  $**p < 0.001$ ,  $***p < 0.0001$ , (hypergeometric test). Cx; Cortex, CA1; hippocampal region CA1, CA3; hippocampal region CA3, DG; dentate gyrus. Bar chart showing RT-qPCR quantification of selected genes de-regulated upon *Neuid* KD in the RNA-seq data ( $n=3$  and  $n=6$ ). Unpaired tTest.

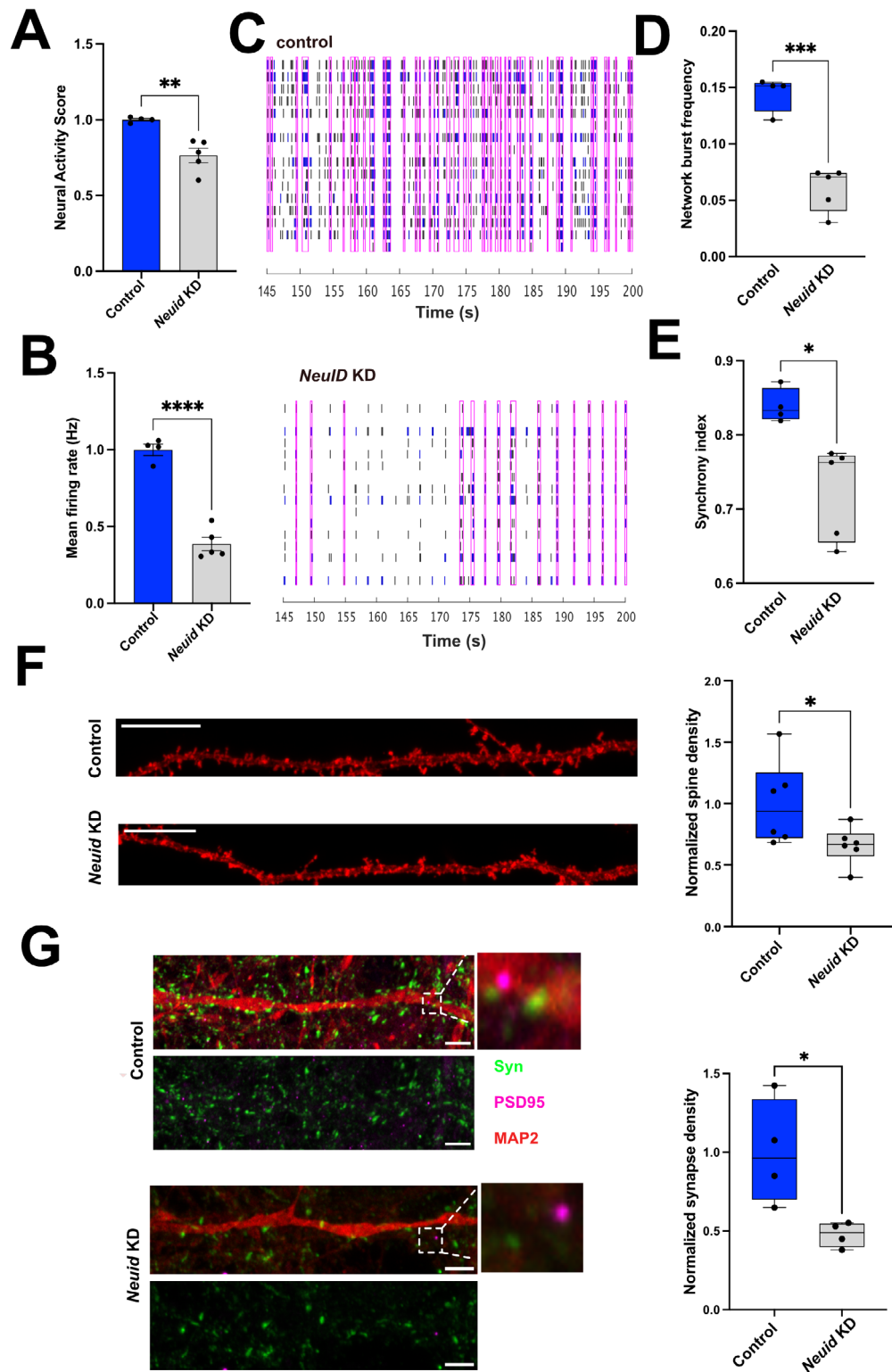


**FIGURE 4** | *NeuId* regulates neuronal activity through modulation of synapses. (A) Bar chart displaying the NAS measured via an MEA assay.  $*p < 0.05$  *NeuID* KD ( $n=4$ ) vs control ( $n=5$ ); Unpaired tTest. (B) Bar plot showing the mean firing rate in control ( $n=4$ ) and *NeuID* KD ( $n=5$ ) conditions.  $****p < 0.0001$ ; Unpaired tTest. (C) Representative raster plots showing neuronal network activity in control ( $n=4$ ) and *NeuID* KD ( $n=5$ ) neurons. (D) Box plot quantifying network burst frequency amongst groups.  $***p < 0.001$  *NeuID* KD vs control; Unpaired tTest. (E) Box plot showing the synchrony index of control vs. *NeuID* neurons.  $*p < 0.05$  *NeuID* KD vs control; Unpaired tTest. (F) Left panel: Representative images showing traced neuronal dendrites stained with DiI dye in control and *NeuID* KD conditions Right panel: Box plot showing normalized dendritic spine density.  $*p < 0.05$  *NeuID* KD vs control; Unpaired tTest. Scale bar 5  $\mu\text{m}$  (G) Left panel: Representative images of synapse quantification via IHC using synaptic markers synaptophysin (syn) and postsynaptic density (PSD-95). Neuron processes are stained with Map2. Scale bar 5  $\mu\text{m}$ . Right panel: Box plot showing the normalized synapse density.  $*p < 0.05$ ; *NeuID* KD vs control; Unpaired tTest. Hz, Herz. Box plots (f,g) show the median (center line) and interquartile range. Data was normalized within each biological replicate and pooled across replicates.

data suggest that neuronal network function is impaired when *Neuid* levels are reduced. We therefore examined the role of *Neuid* in synchronized network burst activity. *Neuid* KD led to sparse electrical activity which is evident from the raster plots showing MEA spike activity in control and *Neuid*-KD neuronal networks (Figure 4c). In these plots, each vertical line represents an action potential (“spike”) detected on a single electrode over time. Dense clusters of vertical lines occurring simultaneously across many electrodes (highlighted by magenta rectangles) correspond to synchronized network bursts, indicating high-frequency firing events involving a large proportion of the network (Figure 4C). *Neuid* KD cultures showed markedly fewer and less coordinated bursts. Quantification of these data confirmed decreased frequency of network bursts upon *Neuid* KD (Figure 4D). Consistent with these findings, the synchronicity index was decreased in *Neuid* KD neurons when compared to the control group (Figure 4e). We confirmed these findings in cortical neurons (Figure S5). These results indicate that decreased levels of *Neuid* impaired spontaneous neuronal firing and impedes synchronized network activity. One possibility to explain these data could be that *Neuid* might be important for maintaining the number and function of physiological synapses within a neuronal network. To test this hypothesis, we employed immunohistochemical approaches to measure synaptic markers informing about the density and number of synapses in response to *Neuid* KD. Our analyses revealed that KD of *Neuid* decreased dendritic spine density (Figure 4f) as measured by DIL dye staining, and led to a reduction in synapse numbers as measured by synaptophysin (Syn) and postsynaptic density 95 (PSD95) costaining (Figure 4g).

Collectively, these data support the view that *Neuid* plays a key role in the regulation of neuronal activity.

### 3.5 | Decreased Levels of *Neuid* Impair Memory Formation in Mice

Our findings suggest that *Neuid* might affect cognitive processes such as memory consolidation. To test this possibility directly, we employed stereotactic injections to administer *Neuid* Gapmer’s into the dorsal hippocampus of wild-type mice and subjected them to a battery of behavioral tests to assess hippocampus-dependent memory formation. To this end, a group of mice was injected into the hippocampus with *Neuid* Gapmer’s or control oligomers, and hippocampal tissue was isolated 2, 4, or 8 days later (Figure 5a). qPCR analysis revealed decreased *Neuid* levels in mice that received *Neuid* Gapmers compared to the control group (Figure 5b). Similar results were obtained when we analyzed the *Neuid* signal by RNAscope in brain sections obtained from mice 4 days after injection (Figure 5c). We also performed qPCR for *Apoe*, which we previously found to be upregulated upon *Neuid* knockdown in primary hippocampal neurons (see Figure 3g). Consistently, the in vivo qPCR data reveal a significant upregulation of *Apoe* expression upon *Neuid* knockdown (Figure 5d). While these data show that *Neuid* levels can be significantly reduced in vivo, it is important to note that stereotactic injection does not affect all hippocampal neurons, which may dilute the overall effect when analyzing whole-tissue extracts. However, previous studies have demonstrated that hippocampus-dependent memory impairment is detectable even

when genes essential for memory formation are disrupted in as little as 10%–20% of all hippocampal neurons [51].

Therefore, we injected another group of mice into the dorsal hippocampus with either *Neuid* Gapmers or control oligonucleotides. Three days later, we subjected them to a fear conditioning paradigm which allows the measurement of contextual and trace fear conditioning, both of which are well-established hippocampus-dependent associative learning tasks (Figure 5a).

During the training session, activity levels and responses to the electric foot shock were similar between groups (Figure 5d). Freezing behavior, a widely used measure of memory consolidation, was significantly impaired in *Neuid* Gapmer-treated mice when tested 24 h after training. The memory test consisted of a re-exposure to the conditioning context (Context A), during which control mice displayed robust freezing, whereas mice injected with *Neuid* Gapmers showed significantly reduced freezing behavior (Figure 5e). This impairment was accompanied by increased locomotor activity during the test session (Figure 5f). Notably, increased locomotor activity during contextual fear testing does not indicate elevated anxiety, as anxiogenic states typically suppress locomotion and increase thigmotaxis in freely moving tasks. Instead, heightened movement during the freezing test is consistent with a failure to maintain the conditioned fear response and therefore reflects impaired memory retrieval rather than altered anxiety levels. Supporting this interpretation, *Neuid* KD mice did not differ from controls in the open field test (Figure S6), indicating that *Neuid* knockdown does not induce anxiety-like behavior.

We observed similar results in the trace fear conditioning test. During training, mice were placed in Context A, and after 3 min, exposed to a tone for 30 s followed by a 15-s trace period during which no stimuli were presented, terminating with a 2-s electric footshock. The tone-trace shock sequence was repeated 3 times, separated by 60-s intertrial (ITI) intervals. Memory recall was tested 24 h later by placing the mice into a novel environment (Context B) and presenting the tone. During the test, freezing behavior significantly increased in both experimental groups in Context B when the tone was played and during the trace period, but decreased during the inter-trial interval (ITI), when no stimulus was present.

*Neuid* Gapmer-treated mice exhibited a significantly impaired freezing response throughout the memory tests (Figure 5g), indicating deficient associative memory. Notably, *Neuid* KD mice failed to show the normal modulation of freezing across tone–trace–ITI blocks that is characteristic of intact associative learning, consistent with impaired stimulus discrimination. This impairment was again accompanied by increased locomotor activity (Figure 5h), further supporting the hypothesis that *Neuid* KD disrupts hippocampus-dependent memory formation.

### 3.6 | CRISPR-Mediated Overexpression of *Neuid* Rescues A $\beta$ -Mediated Loss of Neuronal Plasticity

In summary, our findings provide strong evidence that physiological expression levels of *Neuid* are essential for neuronal plasticity and memory function, while decreased levels are observed in

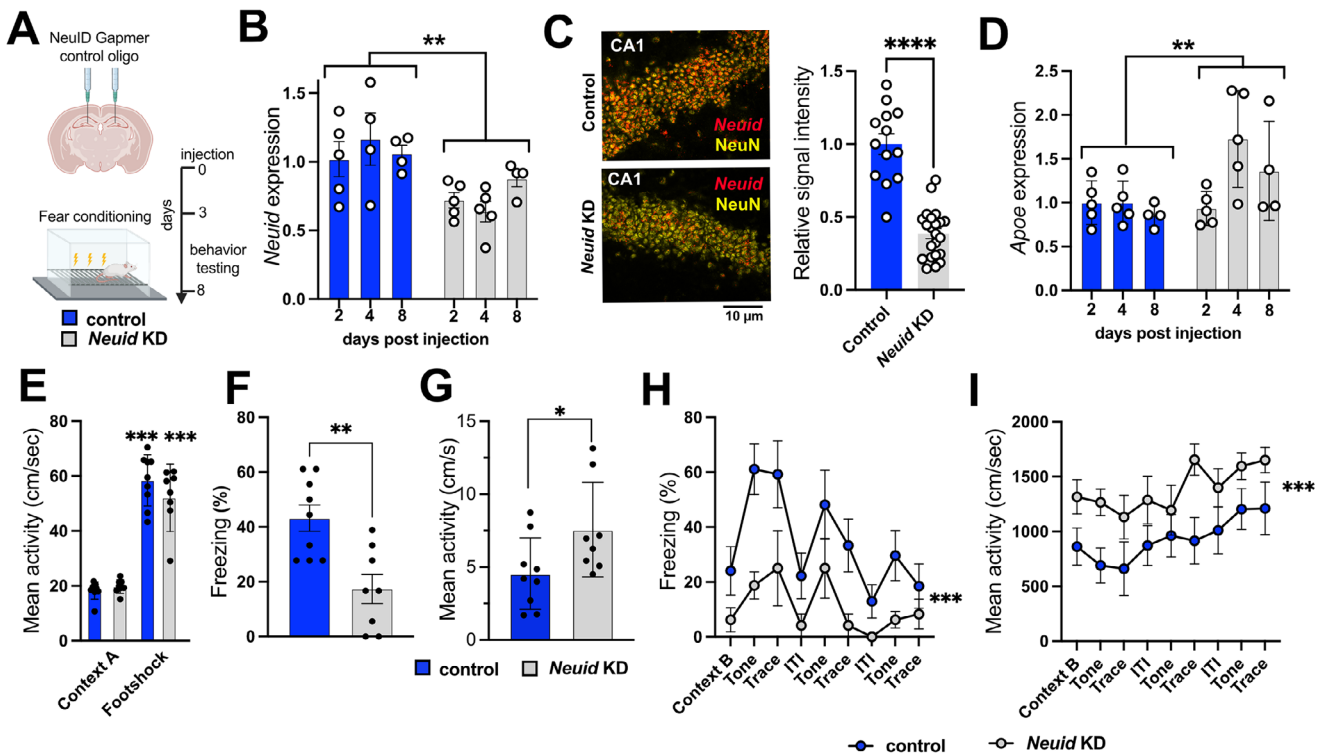


**FIGURE 5** | Decreased levels of *NeuID* impair memory formation in mice. (A) Schematic depiction of experimental design. For the experiment 3 months old mice were used. Behavior testing was performed from day 3–8 after the infection. (B) Bar charts showing qPCR data for *NeuID* expression in the hippocampus of mice, 2, 4, and 8 days after the injection of scrambled oligomers or *NeuID* Gapmer's (*NeuID* knock down ( $n=4-5$ /group)). Two-way ANOVA with factors Treatment (*NeuID* KD vs control) and Time (2, 4, 8 days) showed that treatment had a significant effect,  $**p = 0.0023$ . Neither Time nor the Treatment  $\times$  Time interaction were significant. (C) Left: Representative images from the adult mouse brain sections (3 months old C57Bl/6J mice) showing RNAscope signals for *NeuID* (Red) and neuronal nuclei stained with NeuN (yellow) after the injection of scramble or *NeuID* Gapmers. Right: Bar chart showing Relative intensity quantification in RNAscope between control ( $n = 13$  sections) and *NeuID* gapmer ( $n = 22$  sections) injected mice.  $****p < 0.0001$ , unpaired tTest. (D) Bar charts depicting the expression of *ApoE* in the hippocampus of mice treated as described for (b) ( $n=4-5$ /group). Two-way ANOVA with factors Treatment (*NeuID* KD vs control) and Time (2, 4, 8 days) showed that treatment had a significant effect,  $**p = 0.0095$ . Neither Time nor the Treatment  $\times$  Time interaction were significant. (E) Bar chart depicting the mean activity during the fear conditioning training, indicating that both groups responded similarly to the foot shock (Control,  $n=9$ ; *NeuID* KD,  $n=8$ ).  $***p < 0.0001$  for Context A vs Footshock, unpaired tTest. (F) Bar chart depicting freezing behavior during the memory test (re-exposure to context A).  $**p < 0.01$ , unpaired tTest. A two-way ANOVA including treatment and sex revealed a significant main effect of treatment ( $p = 0.0028$ ), with no significant effect of sex or treatment $\times$ sex interaction. (G) Bar chart depicting the mean activity during the memory test (re-exposure to context A).  $*p < 0.05$ , unpaired tTest. (H) Freezing behavior and mean activity (I) during the memory test for trace fear conditioning. Two-way ANOVA (Treatment  $\times$  Sex) showed a significant main effect of Treatment ( $p = 0.0052$ ), with no main effect of Sex and no Treatment $\times$ Sex interaction for freezing behavior (H) and mean activity (I;  $p = 0.0061$ ). Context B: freezing during re-exposure to context B without presentation of the tone; Tone: freezing during re-exposure to context B during the presentation of the tone; ITI: freezing during the ITI (inter trial interval). Error bars indicate SD.

patients who develop AD. Based on this, we hypothesized that *NeuID* could be a novel drug target for AD.

To test this, we employed neurons treated with amyloid beta ( $A\beta$ ) 42 oligomers as a model system, since our data suggest that *NeuID* expression decreases early in disease progression, and amyloid pathology is widely accepted as one of the earliest molecular changes observed in AD patients [52]. Therefore, we first investigated the effect of  $A\beta$ 42 exposure on *NeuID* expression in primary hippocampal neurons. qPCR analysis, performed 24 h after treatment, revealed that *NeuID* levels were significantly decreased in  $A\beta$ 42-treated neurons compared to the vehicle control group (Figure 6a). Notably, this treatment did not affect neuronal viability, further suggesting that the decreased *NEUID* levels observed in the brains of AD patients do not simply reflect neuronal cell loss (Figure S7). To confirm the efficacy of

$A\beta$ 42 treatment and establish a relevant read out for amyloid pathology, we assessed neuronal activity via MEA recordings. While neuronal activity was similar across all cultures before hippocampal neurons were treated with  $A\beta$ 42 or vehicle control at DIV10, the data have been normalized to these baseline conditions. Recordings were performed 24 h later for 15 min. The data show that  $A\beta$ 42 treatment led to sparse electrical activity (Figure 6b). In agreement with this, the NAS (Figure 6c), the mean firing rate (Figure 6d) and the frequency of network bursts (Figure 6e) were significantly reduced upon  $A\beta$ 42 treatment. These results show that exposure to  $A\beta$ 42 leads to reduced *NeuID* levels and decreased neuronal activity. While the precise mechanisms by which *NeuID* levels decrease remain to be elucidated, acute changes in neuronal activity are unlikely to be the driving force, since treatment of neurons with TTX, bicuculline, or muscimol, using the same experimental conditions as for the

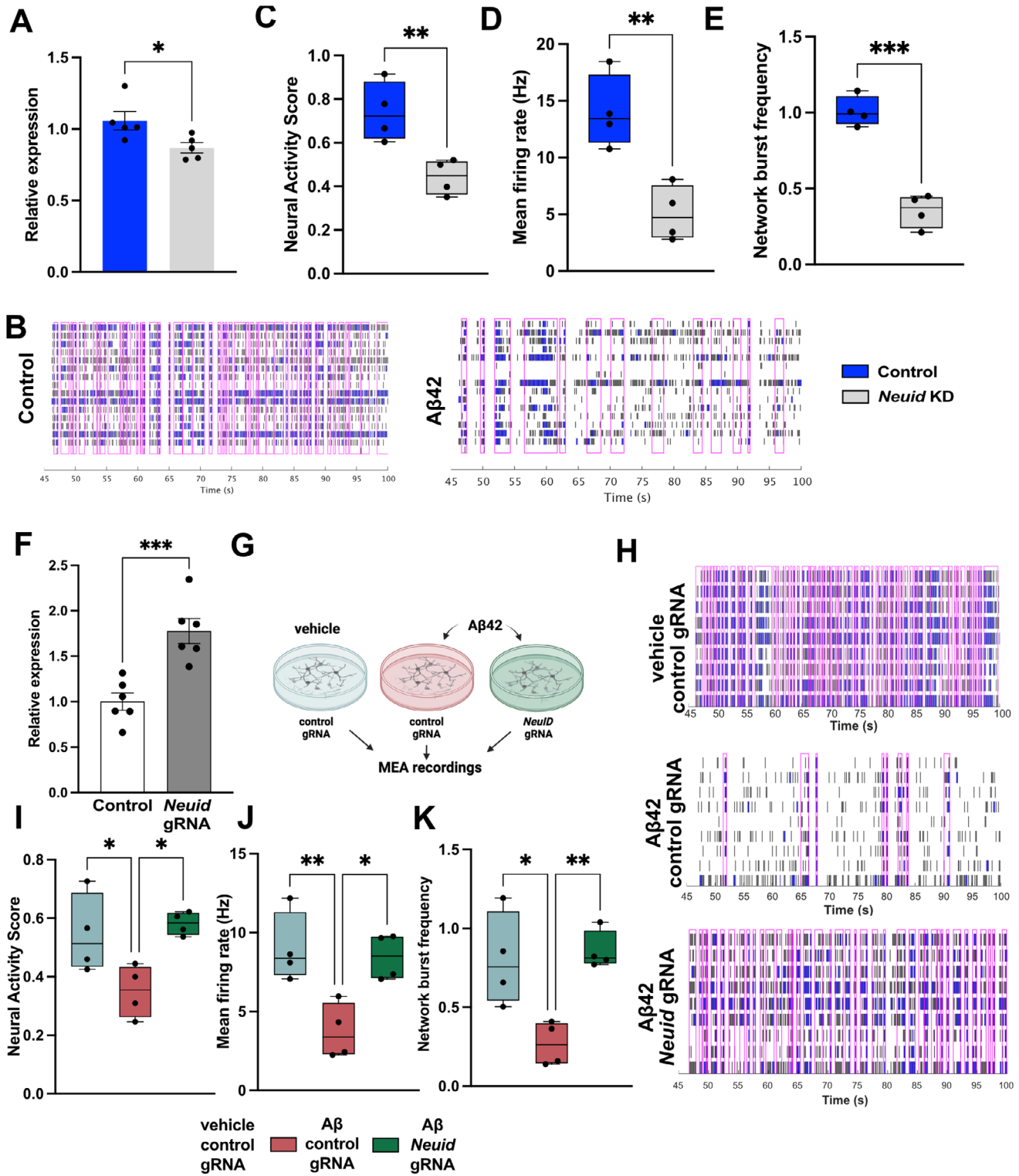


**FIGURE 6** | CRISPRa mediated over-expression of *NeuID* rescues  $A\beta$  mediated neuronal impairment. (A) Bar plot showing the relative expression of *NeuID* in primary hippocampal neurons after treatment with  $A\beta_{42}$  ( $n=5$ ); unpaired tTest  $*p < 0.05$ . (B) Representative raster plots showing electrical activity during MEA recordings in the control and  $A\beta_{42}$  treated groups ( $n=4$ ). (C) Box plots showing the NAS, (D) the mean firing rate and (E) the network burst frequency of hippocampal neurons without (control) and after  $A\beta_{42}$  treatment. (F) Bar plots showing expression of *NeuID* in hippocampal neurons treated with CRISPRa and *NeuID* gRNA (*NeuID* gRNA,  $n=6$ ) and cells that were treated with a control gRNA (control,  $n=6$ ). Cells were transfected at DIV7 and RNA was isolated 48 h later. (G) Experimental scheme for the experiments shown in H–J. (H) Representative raster plots showing electrical activity during MEA recordings of hippocampal neurons that were treated with CRISPRa and either a control gRNA + vehicle (vehicle control gRNA),  $A\beta_{42}$  + control gRNA ( $A\beta_{42}$  control gRNA) or  $A\beta_{42}$  along with the *NeuID* gRNA ( $A\beta_{42}$  *NeuID* gRNA). (I) Box plots showing the NAS, (J) the mean firing rate and (K) the network burst frequency of hippocampal neurons subjected to the experiment described in (g) ( $n=4$ ).  $*p < 0.05$ ,  $**p < 0.01$ ,  $***p < 0.001$ ; unpaired tTest.

A $\beta$ 42 treatment did not significantly alter *Neuid* expression levels (Figure S8).

Having established that MEA recordings provide a suitable readout for amyloid pathology in our experimental setting, we next sought to determine whether increasing *Neuid* levels could reverse these phenotypes. To achieve *Neuid* overexpression, we used the CRISPR-based activation (CRISPRa) method. We generated a guide (g) RNA targeting the *Neuid* promoter, along with a corresponding control gRNA with no target in the genome. To test this approach, primary hippocampal neurons were transfected with the AAVs carrying CRISPRa plasmid together with AAVs containing either scramble or *Neuid*-targeting gRNAs at DIV7, followed by RNA isolation 48 h later. Upon transfection with the CRISPRa plasmid and *Neuid*-targeting gRNA, we observed an approximately onefold increase in *Neuid* expression in primary hippocampal neurons (Figure 6f).

Next, using the same experimental setting we transfected neurons with CRISPRa carrying either the *Neuid* or control gRNA and subjected them to A $\beta$ 42 treatment 48 h after transfection. Neurons transfected with CRISPRa and the control gRNA, but treated only with the vehicle, served as an additional control (Figure 6g). We confirmed that A $\beta$ 42 reduces *Neuid* expression and that CRISPRa-mediated activation restores *Neuid* levels (Figure S9A). MEA analysis revealed that CRISPRa-mediated *Neuid* overexpression rescued the A $\beta$ 42-mediated defects in electrical activity (Figure 6h), NAS (Figure 6i), mean firing rate (Figure 6j) and frequency of network bursts (Figure 6k). Since expression changes in *Neuid* did not have a direct effect on A $\beta$ 42 (Figure S9B), these findings suggest that increasing *Neuid* expression could serve as a novel therapeutic strategy for AD.

### 3.7 | NeuID Interacts with EZH2 Methyltransferase and Regulates the Expression of Olig2 Transcription Factor

Finally, we wanted to elucidate the mechanisms by which *Neuid* regulates neuronal function. Previous data have shown that nuclear lncRNAs can contribute to gene expression control by binding to regulatory elements on DNA, such as promoter regions, while simultaneously interacting with transcriptional regulators, including chromatin-modifying enzymes [30, 53, 54]. Through this mode of action, lncRNAs can either recruit transcriptional regulators to specific genomic locations or act as molecular decoys [55–57]. To explore if such a mode of action may apply to *Neuid*, we employed Enrichr, an integrative tool that compiles multiple gene-set libraries to identify gene-regulatory mechanisms [58]. This analysis revealed that genes deregulated upon *Neuid* knock down are likely controlled, at least in part, by EZH2 (Figure 7a). EZH2 is a subunit of the Polycomb Repressive Complex 2 (PRC2) that mediates gene-repression via histone 3 lysine 27 trimethylation (H3K27me3). Previous studies have shown that lncRNAs can recruit PRC2 to specific chromatin locations to silence gene-expression [30, 59]. Moreover, reduced EZH2 function in the adult brain has been linked to the loss of neuronal identity and neurodegenerative phenotypes [60]. EZH2 was shown to bind the lncRNA HOX antisense intergenic RNA (*Hotair*) [61]. The identified binding region contains short guanine repeats that fold into guanine

quadruplexes (G-quadruplexes) which are essential for RNA-protein interactions [61]. Therefore, the nucleotide sequences from mouse *Neuid* and human *NEUID* variants were screened for G-quadruplex and i-motifs using G4Boost [62] and iM-seeker [63]. While no i-motifs could be detected, we detected one similar G-quadruplex motif which is similar to the reported EZH2 binding site within *Hotair* (Figure 7b). These data suggests that *Neuid* may interact with the PRC2 complex and more specifically with EZH2. To test this, we performed RNA immunoprecipitation (RNA-IP) using an EZH2-targeting antibody, with an IgG isotype antibody serving as a control. Following immunoprecipitation, RNA was isolated from the IP fractions, and *Neuid* levels were quantified via qPCR. *Neuid* enrichment in the EZH2 or IgG IP fractions is shown as the percentage of *Neuid* transcripts in the IP relative to the corresponding input fractions. This experiment confirmed that *Neuid* binds to EZH2, as *Neuid* was specifically enriched in the EZH2 IP compared to the IgG control (Figure 7c). In the case of *Hotair* it was shown that its binding to EZH2 regulates its ability to maintain H3K27me3 thereby helping to maintain gene-expression control [64]. Therefore, we hypothesized that KD of *Neuid* might alter neuronal H3K27me3 levels, which could help explain the increased expression of non-neuronal genes observed upon *Neuid* KD. To explore this hypothesis, we performed H3K27me3 ChIP-sequencing on primary hippocampal neurons treated with either control or *Neuid* Gapmers. Principal component analysis (PCA) revealed that neuronal H3K27me3 patterns are affected by *Neuid* KD (Figure 7d).

Next, we performed a differential binding analysis to identify H3K27me3 peaks that significantly differed between control and *Neuid* KD neurons. Our differential binding analysis revealed 854 genes with decreased H3K27me3 and 645 genes with increased H3K27me3 upon *Neuid* knockdown (KD) (FDR < 0.1; |FC| > 1; see Table S7 and Figure S10). A GO term analysis of genes with altered H3K27me3 indicated enrichment for developmental programs. Importantly, GO term enrichment among genes with decreased H3K27me3 was more significant than that among genes that gain H3K27me3, highlighting processes such as “cell differentiation” and “central nervous system development.” These findings are consistent with our other results suggesting that loss of *Neuid* compromises EZH2 function, leading to reduced H3K27me3 at genes linked to early developmental programs, which subsequently become upregulated and disrupt neuronal homeostasis (Figure S10).

We then intersected the genes showing decreased H3K27me3 in ChIP-seq (Figure 7E) with the transcripts that were significantly upregulated upon *Neuid* KD in RNA-seq, and identified 31 genes that exhibited reduced H3K27me3 occupancy and were significantly upregulated following *Neuid* KD (Figure 7f; Figure S10). These genes are bona fide candidates to be directly regulated by *Neuid* acting through the PRC2 complex. GO term analysis of these genes revealed that they represent developmental processes such as “brain development”, “neurogenesis” and “regulation of neuronal differentiation” (Figure 7G; Table S8). Upon closer inspection of the genes that exhibit decreased H3K27me3 binding and increased expression upon *Neuid* knock down, we detected 4 key transcription factors linked to neurodevelopmental processes and that are specific to glial cells under physiological conditions in the adult brain, namely *Etv5*, *Hes1*, *Olig2*, and *Tcf12* (Figure 7h; Figures S10C and S11). Therefore we hypothesized that the

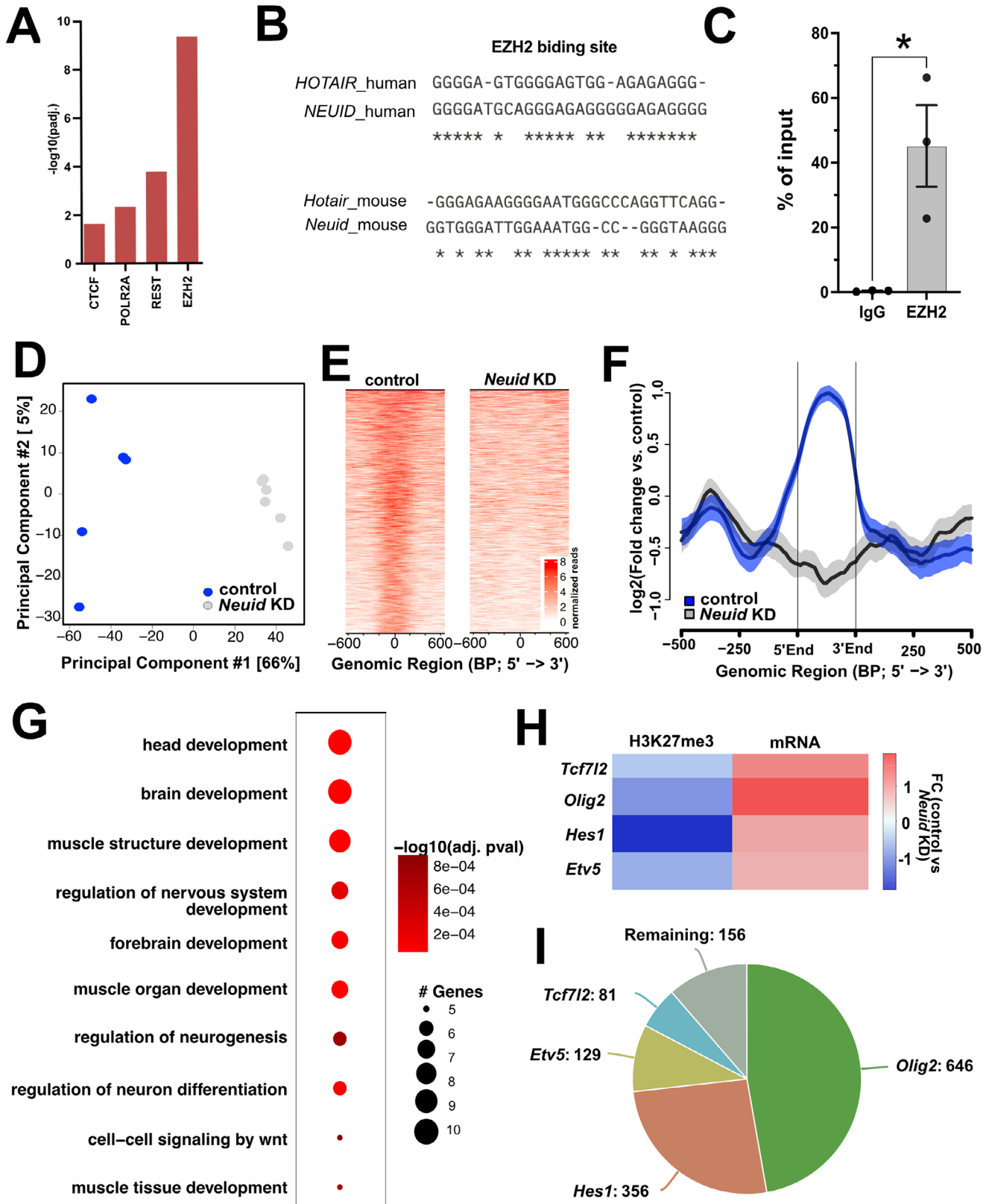


**FIGURE 7** | *Neuid* interacts with the EZH2 and affects H3K27 methylation of non-neuronal genes in neurons (A) EnrichR analysis using the genes de-regulated upon *Neuid* knock down as input reveals *EZH2* as a potential interaction partner for *Neuid*. (B) Sequence comparison of the reported *EZH2* binding region within the lncRNA *Hotair* to *Neuid* in mouse and humans reveals strong similarity. (C) Bar graph depicting the results from RNA-immunoprecipitation qPCR showing the interaction of *Neuid* with *EZH2*. *Neuid* qPCR was performed in RNA obtained from anti-*EZH2* or IgG control IP fractions. *Neuid* binding to *EZH2* or IgG is quantified with the % input method, where the amount of *Neuid* bound to *EZH2* or IgG is quantified as a percentage of *Neuid* present in input fractions. unpaired tTest \* $p < 0.05$ . (D) Principal component analysis showing the results for H3K27me3 ChIP-seq in neurons upon *Neuid* knock down in comparison to control ( $n = 5$ /group) (E) Heatmap showing H3K27me3 occupancy across the 854 genes identified as

increased expression of the four transcription factors may help explain, at least in part, the differential expression of genes that were upregulated following *NeuID* knockdown. To test this, we performed a promoter region analysis to determine how many of the 892 genes upregulated upon *NeuID* knockdown contained promoter binding sites for *Etv5*, *Hes1*, *Olig2*, and/or *Tcf7l2*. The data revealed that the majority of these genes can be regulated by *Olig2* (646), followed by *Hes1* (356), *Etv5* (129), and *Tcf7l2* [81] (Figure 7I). A combined analysis of the predicted target genes of the four transcription factors showed that in total 734 (84%) of the 892 upregulated genes could potentially be explained by increased activity of these factors (Figure 7i; Table S9). A small subset of genes ( $n = 8$ ) exhibited increased H3K27me3 together with reduced expression upon *NeuID* KD. Because these genes did not cluster into any coherent functional category, they are unlikely to account for the broader transcriptional downregulation observed upon *NeuID* knockdown. Instead, the 597 downregulated genes most likely reflect secondary transcriptional consequences of impaired neuronal homeostasis, rather than direct primary targets of *NeuID*-dependent H3K27me3 regulation (Figure S10D).

#### 4 | Discussion

In this study, we report the discovery and first functional characterization of *NeuID*, a previously unstudied, neuron-specific, and brain-enriched lncRNA. Through integrative transcriptomic analysis across human and mouse datasets, we identified *NEUID* as one of the few lncRNAs that is conserved, enriched in the brain, and selectively expressed in neuronal populations. We have previously used this approach to identify lncRNAs in other cell types relevant to AD pathology. For example, we characterized the astrocyte-specific lncRNA *PRDM16-DT* and demonstrated its functional relevance in AD [8, 11, 30, 65, 66]. These findings are in line with previous data reporting roles for lncRNAs in AD pathogenesis such as *BACE1-AS*, *BDNF-AS* or *MEG3* [14] are likely to support further discovery of lncRNAs involved in neurodegeneration, emphasizing the utility of our strategy in exploring the lncRNAome for therapeutic targets.

*NEUID* is significantly downregulated in three independent cohorts of AD brain samples, and its expression inversely correlates with B&B staging, suggesting a role in early disease progression. To date, our analyses rely on bulk tissue expression data and the qPCR cohort is rather small. Future studies should therefore assess *NEUID* expression in a cell type-specific manner using absolute quantification approaches, such as laser-capture microdissection followed by digital PCR. Importantly, *NeuID* levels are also reduced in response to A $\beta$ 42 in vitro, under conditions that do not readily induce neurodegeneration, while *NEUID* levels are not altered in FTD, indicating that *NEUID* loss is not merely a secondary effect of neuronal cell death. Future research should aim to elucidate the precise mechanisms

leading to A $\beta$ 42-mediated downregulation of *NEUID* and to determine whether other AD risk factors also alter *NEUID* expression.

Mechanistically, our data suggest that *NeuID* operates through an epigenetic axis involving the PRC2 complex. We show that *NeuID* interacts with EZH2, affecting H3K27me3 levels at loci associated with developmental and glial-specific genes. This is consistent with previous studies demonstrating that the lncRNA *Hotair* recruits EZH2 to specific chromatin regions to direct H3K27me3 deposition [61, 64]. Supporting a similar mechanism for human and mouse *NEUID/NeuID*, we identified a conserved EZH2-binding motif within its sequence, homologous to the EZH2 interaction domain in *Hotair*.

Notably, *NeuID* loss does not lead to a global reduction of PRC2 activity, but instead results in a selective derepression of developmental and glial gene programs, while other genes remain largely unaffected. This suggests that *NeuID* confers locus- and context-specific guidance to PRC2 in neurons, stabilizing H3K27me3-mediated repression at regulatory regions that must remain silenced to preserve neuronal identity.

While we cannot exclude that *NeuID* has additional binding partners and that future research should address the DNA, RNA, and protein interactions of *NeuID* in a context-specific manner, our findings support the emerging hypothesis that cell-type-specific lncRNAs orchestrate the activity of ubiquitously expressed chromatin regulators such as EZH2, thereby maintaining cellular identity. This concept, previously proposed in other systems [67–69], is here extended to the context of neuronal identity and neurodegeneration. In line with this model, we have previously shown that the astrocyte-specific lncRNA *PRDM16-DT* also interacts with EZH2 but functions as a molecular recruiter to establish astrocyte-specific chromatin states [30], highlighting that distinct cell-type-restricted lncRNAs can tune PRC2 activity in mechanistically different ways to reinforce lineage identity.

In *NeuID*-deficient neurons, we observed derepression of 892 genes, many involved in developmental or glial pathways, consistent with a loss of neuronal identity. Among them, 62 genes showed decreased H3K27me3 occupancy, suggesting direct regulation by *NeuID*. These 62 genes were enriched for developmental and glial-specific pathways, and notably included key transcription factors such as *Olig2*, *Etv5*, *Tcf7l2*, and *Hes1*, which are important for brain development and are linked to glia cell function in the adult brain [70–73]. Our motif analysis indicates that these transcription factors may explain up to 85% of secondary transcriptional changes observed upon *NeuID* KD, further supporting the view that a key function of *NeuID* is to orchestrate the silencing of non-neuronal genes in neurons by guiding the PRC2 complex. Future studies combining high-resolution chromatin

---

having significantly reduced H3K27me3 levels. (F) NGS plot showing the distribution of H3K27me3 along the 31 genes up-regulated upon *NeuID* knockdown showing significantly decreased H3K27me3 levels. G. Dot blot showing significantly enriched GO terms from the 31 genes depicted in (F). (H) Heat map showing H3K27me Chip-seq and mRNA levels detected via RNA-seq signals for key transcription factors normally specific to glial cells. Depicted is the log<sub>2</sub>FC value. (I) Venn diagram showing the overlap of genes upregulated upon *NeuID* knockdown that are predicted targets of each of the displayed transcription factors. Note that out of 892 upregulated genes, only 154 could not be explained by the four transcription factors. Error bars show SEM.

---

profiling with RNA-centered proximity-labeling approaches will be required to define the precise genomic binding sites and interaction partners of *Neuid* and to further dissect how neuronal lncRNAs selectively modulate PRC2 activity.

Furthermore, these data imply that *Neuid* functions as a molecular recruiter of PRC2 to the promoter of non-neuronal target genes. This contrasts with the recently described lncRNA *PRDM16-DT*, which interacts with PRC2 as a decoy, blocking its activity to preserve astrocyte identity. Together, these findings suggest that in the brain, one function of nuclear, cell-type-specific lncRNAs may be to either guide or prevent PRC2 activity to maintain the correct cell-type specific epigenetic landscape. Clearly more research is needed to further test this hypothesis for PRC2 and other chromatin modifying complexes.

Loss of *Neuid* not only altered gene expression but also disrupted neuronal physiology. We observed reduced dendritic spine density, fewer synapses, impaired neuronal network synchronization, and deficits in hippocampus-dependent memory, which was accompanied by decreased expression of genes linked to neuronal plasticity. This is in line with previous studies showing that manipulation of lncRNAs can affect neuronal plasticity and memory function [7, 74, 75]. Since we did not observe evidence that *Neuid* directly regulates these genes, we suggest that the loss of neuronal function and the downregulation of genes related to neuronal plasticity is a secondary effect, reflecting the consequences of neurons entering a developmental and glial cell-specific gene expression program.

Notably, *Neuid* was downregulated by  $A\beta$ 42 exposure, a hallmark of early AD pathology, and CRISPRa-mediated overexpression of *Neuid* restored physiological expression levels and reinstated  $A\beta$ 42-induced defects in neuronal network activity. To the best of our knowledge, this is the first time such an effect is described for a neuronal lncRNA, although previous studies have reported that lncRNAs can exhibit altered expression in models for amyloid pathology [14, 76, 77]. Importantly, since *Neuid* overexpression was performed before  $A\beta$ 42 exposure, the observed effects should be interpreted as protective rather than therapeutic, and additional in vivo studies will be necessary to test whether *Neuid* can rescue pathology once it is already established.

Although we show that *Neuid* regulates H3K27me3 via EZH2, the broader epigenetic impact of *Neuid* remains incompletely mapped. Many of the transcriptional changes observed upon *Neuid* KD are likely indirect. This view is supported by our finding that, out of the 892 upregulated genes, only 62 may be directly regulated by *Neuid* through its interaction with EZH2. Notably, among these 62 genes were key transcription factors that could account for up to 85% of the upregulated genes following *Neuid* KD. Most prominent was OLIG2, which is consistent with previous studies showing that elevated levels of OLIG2 in neural progenitor cells are linked to the pathogenesis of Down syndrome, an intellectual disability disorder associated with beta amyloid pathology [78, 79].

As this is the first report of *Neuid* there are several other key questions to be addressed in future research. For example, the mechanisms governing *Neuid*'s neuron-specific expression remain not well understood. It may also be worth exploring

whether *Neuid* becomes upregulated in non-neuronal cell types under pathological conditions. In this context, testing whether ectopic *Neuid* expression in glial cells can repress glia-specific gene programs would be particularly interesting. To determine whether *Neuid* serves similar functions in different neuronal subtypes (e.g., inhibitory versus excitatory neurons) would be an important direction for future research. In addition, it would be interesting to elucidate how AD risk factors such as  $A\beta$ 42 downregulate *Neuid* and eventually the therapeutic potential for targeting *Neuid* needs to be tested in animal models and human iPSC derived cells. It is also interesting to note an unreviewed UniProt entry (Q3URA8) lists Gm10419 (*NEUID*) as a hypothetical small protein. While this prediction dates from 2005, lacks experimental support and modern annotation databases (Ensembl, GENCODE) classify *Gm10419* (*NEUID*) as a lncRNA, it cannot be fully excluded that under specific conditions *NEUID* may be translated.

From a medical translational perspective, it would also be important to assess *NEUID* expression in liquid biopsies from patients at various stages of AD pathogenesis. The analysis of non-coding RNAs (ncRNAs) as biomarkers for AD is an active area of research, particularly in the case of microRNAs [80–82]. However, emerging data also support the view that analyzing lncRNAs in blood may represent a promising strategy for the development of novel biomarkers in AD [83, 84]. This could support the development of stratified therapies towards lncRNA expression and/or function that might be applied in combination with other approaches, such as anti-amyloid-based treatments. In this context, it will also be important to conduct future in vivo studies in AD mouse models to assess whether activation of *Neuid* can ameliorate neuronal dysfunction and cognitive deficits.

From a translational perspective, RNA-based targeting of *Neuid*/*NEUID* will require careful consideration of delivery, target engagement, and safety in the central nervous system. Although efficient brain delivery remains challenging, clinically validated strategies already exist. In particular, intrathecal administration of antisense oligonucleotides (ASO), as established for Nusinersen (to treat spinal muscle ataxia) or Tofersen (to treat amyotrophic lateral sclerosis), enables durable neuronal target engagement with infrequent dosing and has demonstrated safety in human CNS [85, 86]. Clinical trials to target AD-associated proteins Tau and APP are ongoing (NCT05399888; NCT05231785). In parallel, emerging approaches such as receptor-mediated blood–brain barrier shuttles, intranasal delivery, and optimized RNA chemistries may further expand the therapeutic window for lncRNA-based interventions [87, 88]. Given the strict neuronal specificity and nuclear mode of action of *NEUID*, targeted activation strategies may minimize off-target effects in non-neuronal tissues. Future in vivo studies will be required to assess delivery efficiency, durability, and long-term safety in AD models.

In summary, our findings identify *Neuid* as a critical regulator of neuronal identity and plasticity, with direct implications for AD. Its strict neuronal specificity and defined mechanism of action position it at the intersection of epigenetic control, synaptic integrity, and memory function, making it a compelling and precise target for RNA-based therapeutic strategies in neurodegeneration.

## Author Contributions

R.P. conducted most of the experiments, analyzed data and generated figures. Z.P. and J.R. performed stereotactic injection and performed behavioral experiments. M.S.S. and I.F. contributed to the initial discovery of Neuid. V.G. performed FANS. S.S. performed RNAscope. D.M.K. and T.P. contributed to the bioinformatic analysis. E.D. performed DIL dye staining. T.D.S., K.B., and I.D. analyzed the FHS data and I.D. provided postmortem brain tissue. K.T. provided human heart biopsies and S.B., A.L.S. and F.S. performed RNAseq experiments. A.F. conceived and supervised the project.

## Acknowledgements

R.P., M.S.S., and E.D. are students of the IMPRS Neuroscience programme (University Göttingen) and S.S. is a student of the IMPRS Genome Science Programme (University Göttingen). V.G. is a student of the International Max Planck Research School for Genome Science.

Open access funding enabled and organized by Projekt DEAL.

## Funding

A.F. was supported by the DFG (Deutsche Forschungsgemeinschaft) SFB1286 and GRK2824; The German Federal Ministry of Science and Education (BMBF) via the ERA-NET Neuron project EPINEURODEVO; The EU Joint Programme- Neurodegenerative Diseases (JPN-D)—EPI-3E; Germany's Excellence Strategy—EXC 2067/1 390729940. A.F. and V.G. were supported by the DFG graduate school GRK2824. F.S. was supported by the GoBIO project miRassay (16LW0055) by the German Federal Ministry of Science and Education. I.D., J.K.B. and T.D.S. were supported by NIH RFIAG078299. TDS and JKB are supported by NIH grants P30AG072978 and U19AG068753. J.K.B. was supported by NIH grant RFIAG078299 and T.D.S. received funding from the National Heart, Lung and Blood Institute (N01-HC-25195, 75N92019D00031 and HHSN268201500001) and the United States Department of Veterans Affairs, Veterans Health Administration, BLRD Merit Award I01BX005933 (T.D.S.). J.S. was supported by project R01MH108837 (NIH/NIMH).

## Conflicts of Interest

The authors declare no conflicts of interest.

## Data Availability Statement

RNA Sequencing data is available via GEO accession GSE296334. ChIP-seq data is available via GSE296334. The human snucRNAseq is from (30).

## References

1. K. D. Warner, C. E. Hajdin, and K. M. Weeks, "Principles for Targeting RNA With Drug-Like Small Molecules," *Nature Reviews Drug discovery* 17, no. 8 (2018): 547–558, <https://doi.org/10.1038/nrd.2018.93>.
2. J. S. Mattick, P. P. Amaral, P. Carninci, et al., "Long Non-coding RNAs: Definitions, Functions, Challenges and Recommendations," *Nature Reviews Molecular Cell Biology* 24, no. 6 (2023): 430–447, <https://doi.org/10.1038/s41580-022-00566-8>.
3. W. S. Liao, S. Samaddar, S. Banerjee, and T. W. Bredy, "On the Functional Relevance of Spatiotemporally-specific Patterns of Experience-dependent Long Noncoding RNA Expression in the Brain," *RNA Biology* 18, no. 7 (2020): 1025–1036, <https://doi.org/10.1080/15476286.2020.1868165>.
4. L. Statello, C. J. Guo, L. L. Chen, and M. Huarte, "Gene Regulation by Long Non-coding RNAs and Its Biological Functions," *Nature Reviews Molecular Cell Biology* 22, no. 2 (2021): 96–118, <https://doi.org/10.1038/s41580-020-00315-9>.
5. T. Derrien, R. Johnson, G. Bussotti, et al., "The GENCODE v7 Catalog of human Long Noncoding RNAs: Analysis of Their Gene Structure,

- Evolution, and Expression," *Genome Research* 22, no. 9 (2012): 1775–1789, <https://doi.org/10.1101/gr.132159.111>.
6. J. A. Briggs, E. J. Wolvetang, J. S. Mattick, J. L. Rinn, and G. Barry, "Mechanisms of Long Non-coding RNAs in Mammalian Nervous System Development, Plasticity, Disease, and Evolution," *Neuron* 88, no. 5 (2015): 861–877, <https://doi.org/10.1016/j.neuron.2015.09.045>.
  7. I. Espadas, J. L. Wingfield, Y. Nakahata, et al., "Synaptically-targeted Long Non-coding RNA SLAMR Promotes Structural Plasticity by Increasing Translation and CaMKII Activity," *Nature Communications* 15, no. 1 (2024): 2694, <https://doi.org/10.1038/s41467-024-46972-8>.
  8. T. Zhang, P. Pang, Z. Fang, et al., "Expression of BCI Impairs Spatial Learning and Memory in Alzheimer's Disease Via APP Translation," *Molecular Neurobiology* 55, no. 7 (2018): 6007–6020, <https://doi.org/10.1007/s12035-017-0820-z>.
  9. J. Yi, B. Chen, X. Yao, Y. Lei, F. Ou, and F. Huang, "Upregulation of the lncRNA MEG3 Improves Cognitive Impairment, Alleviates Neuronal Damage, and Inhibits Activation of Astrocytes in Hippocampus Tissues in Alzheimer's disease Through Inactivating the PI3K/Akt Signaling Pathway," *Journal of Cellular Biochemistry* 120, no. 10 (2019): 18053–18065, <https://doi.org/10.1002/jcb.29108>.
  10. P. Ma, Y. Li, W. Zhang, et al., "Long Non-coding RNA MALAT1 Inhibits Neuron Apoptosis and Neuroinflammation While Stimulates Neurite Outgrowth and Its Correlation with MiR-125b Mediates PTGS2, CDK5 and FOXQ1 in Alzheimer's Disease," *Current Alzheimer Research* 16, no. 7 (2019): 596–612, <https://doi.org/10.2174/1567205016666190725130134>.
  11. S. Balusu, K. Horré, N. Thrupp, et al., "MEG3 Activates Necroptosis in Human Neuron Xenografts Modeling Alzheimer's Disease," *Science* 381, no. 6683 (2023): 1176–1182, <https://doi.org/10.1126/science.abp9556>.
  12. M. Winkle, S. M. El-Daly, M. Fabbri, and G. A. Calin, "Noncoding RNA Therapeutics — Challenges and Potential Solutions," *Nature Reviews Drug Discovery* 20, no. 8 (2021): 629–651, <https://doi.org/10.1038/s41573-021-00219-z>.
  13. T. R. Damase, R. Sukhovshin, C. Boada, F. Taraballi, R. I. Pettigrew, and J. P. Cooke, "Frontiers in Bioengineering and Biotechnology," *Frontiers in Bioengineering and Biotechnology* 9 (2021): 628137, <https://doi.org/10.3389/fbioe.2021.628137>.
  14. M. A. Faghihi, F. Modarresi, A. M. Khalil, et al., "Expression of a Noncoding RNA is Elevated In Alzheimer's Disease and Drives Rapid Feed-Forward Regulation of  $\beta$ -Secretase," *Nature Medicine* 14, no. 7 (2008): 723–730, <https://doi.org/10.1038/nm1784>.
  15. M. Magistri, D. Velmeshev, M. Makhmutova, and M. A. Faghihi, "Transcriptomics Profiling of Alzheimer's Disease Reveal Neurovascular Defects, Altered Amyloid- $\beta$  Homeostasis, and Deregulated Expression of Long Noncoding RNAs," *Journal of Alzheimer's Disease* 48, no. 3 (2015): 647–665, <https://doi.org/10.3233/JAD-150398>.
  16. M. Zhou, H. Zhao, X. Wang, J. Sun, and J. Su, "Analysis of long noncoding RNAs highlights region-specific altered expression patterns and diagnostic roles in Alzheimer's disease," *Briefings in Bioinformatics* 20, no. 2 (2019): 598–608, <https://doi.org/10.1093/bib/bby021>.
  17. B. De Strooper and E. Karran, "The Cellular Phase of Alzheimer's Disease," *Cell and Tissue Research* 164, no. 4 (2016): 603–615.
  18. D. P. Veitch, M. W. Weiner, M. Miller, et al., "The Alzheimer's Disease Neuroimaging Initiative in the Era of Alzheimer's Disease Treatment: A Review of ADNI Studies From 2021 to 2022," *Alzheimer's & Dementia* 20, no. 1 (2024): 652–694, <https://doi.org/10.1002/alz.13449>.
  19. J. Zhang, Y. Zhang, J. Wang, Y. Xia, J. Zhang, and L. Chen, "Recent advances in Alzheimer's disease: Mechanisms, clinical trials and new drug development strategies," *Signal Transduction and Targeted Therapy* 9, no. 1 (2024): 211, <https://doi.org/10.1038/s41392-024-01911-3>.
  20. L. Wang, K. R. Bharti, P. F. Pavlov, and B. Winblad, "Small Molecule Therapeutics for Tauopathy in Alzheimer's Disease: Walking on the Path of Most Resistance," *European Journal of Medicinal Chemistry* 209 (2021): 112915.

21. M. T. Heneka, W. M. van der Flier, F. Jessen, et al., “Neuroinflammation in Alzheimer Disease,” *Nature Reviews Immunology* 25, no. 5 (2025): 321–352, <https://doi.org/10.1038/s41577-024-01104-7>.
22. J. L. Cummings, A. M. L. Osse, J. W. Kinney, D. Cammann, and J. Chen, “Alzheimer’s Disease: Combination Therapies and Clinical Trials for Combination Therapy Development,” *CNS Drugs* 38, no. 8 (2024): 613–624, <https://doi.org/10.1007/s40263-024-01103-1>.
23. K. Anthony, “RNA-based Therapeutics for Neurological Diseases,” *RNA Biology* 19, no. 1 (2022): 176–190, <https://doi.org/10.1080/15476286.2021.2021650>.
24. I. Brentari, M. Zadorozhna, M. A. Denti, and E. Giorgio, “RNA Therapeutics for Neurological Diseases,” *British Medical Bulletin* 147, no. 1 (2023): 50–61, <https://doi.org/10.1093/bmb/ldad010>.
25. R. Panitch, J. Hu, W. Xia, et al., “Blood and Brain Transcriptome Analysis Reveals APOE Genotype-mediated and Immune-Related Pathways Involved in Alzheimer Disease,” *Alzheimer’s Research & Therapy* 14, no. 1 (2022): 30, <https://doi.org/10.1186/s13195-022-00975-z>.
26. T. Berulava, E. Buchholz, V. Elerdashvili, et al., “Changes in m6A RNA Methylation Contribute to Heart Failure Progression by Modulating Translation,” *European Journal of Heart Failure* 22, no. 1 (2020): 54–66, <https://doi.org/10.1002/ejhf.1672>.
27. V. Jovasevic, H. Zhang, F. Sananbenesi, et al., “Primary Cilia Are Required for the Persistence of Memory and Stabilization of Perineuronal Nets,” *Science* 24, no. 6 (2021): 102617.
28. M. S. Sakib, G. Sokpor, H. P. Nguyen, A. Fischer, and T. Tuoc, “Intranuclear Immunostaining-based FACS Protocol From Embryonic Cortical Tissue,” *Star Protocols* 2, no. 1 (2021): 100318, <https://doi.org/10.1016/j.xpro.2021.100318>.
29. A. Michurina, M. S. Sakib, C. Kerimoglu, et al., “Postnatal Expression of the Lysine Methyltransferase SETD1B is Essential for Learning and the Regulation of Neuron-Enriched Genes,” *The EMBO Journal* 41, no. 1 (2022): 106459, <https://doi.org/10.15252/embj.2020106459>.
30. S. Schröder, U. Fuchs, V. Gisa, et al., “PRDM16-DT is a Novel lncRNA that Regulates Astrocyte Function in Alzheimer’s Disease,” *Acta Neuropathologica* 148, no. 1 (2024): 32, <https://doi.org/10.1007/s00401-024-02787-x>.
31. M. I. Love, W. Huber, and S. Anders, “Moderated Estimation of Fold Change and Dispersion for RNA-seq Data with DESeq2,” *Genome Biology* 15, no. 1 (2014): 550, <https://doi.org/10.1186/s13059-014-0550-8>.
32. J. Feng, T. Liu, B. Qin, Y. Zhang, and X. S. Liu, “Identifying ChIP-seq Enrichment Using MACS,” *Nature Protocols* 7, no. 9 (2012): 1728–1740, <https://doi.org/10.1038/nprot.2012.101>.
33. T. M. R. Noviello, A. Di Liddo, G. M. Ventola, et al., “Detection of long non-coding RNA homology, a comparative study on alignment and alignment-free metrics,” *BMC Bioinformatics [Electronic Resource]* 19, no. 1 (2018): 407, <https://doi.org/10.1186/s12859-018-2441-6>.
34. L. Lorenzi, H.-S. Chiu, F. Avila Cobos, et al., “The RNA Atlas Expands the Catalog of Human Non-Coding RNAs,” *Nature Biotechnology* 39, no. 11 (2021): 1453–1465, <https://doi.org/10.1038/s41587-021-00936-1>.
35. H. B. E. Braak, “Staging of Alzheimer’s Disease-related Neurofibrillary Changes,” *Neurobiology of Aging* 16 (1995): 271–278, [https://doi.org/10.1016/0197-4580\(95\)00021-6](https://doi.org/10.1016/0197-4580(95)00021-6).
36. R. Panitch, J. Hu, J. Chung, et al., “Integrative Brain Transcriptome Analysis Links Complement Component 4 and HSPA2 to the APOE  $\epsilon$ 2 Protective Effect in Alzheimer Disease,” *Molecular Psychiatry* 26, no. 10 (2021): 6054–6064, <https://doi.org/10.1038/s41380-021-01266-z>.
37. K. Menden, M. Francescato, T. Nyima, et al., “A Multi-omics Dataset for the Analysis of Frontotemporal Dementia Genetic Subtypes,” *Scientific Data* 10, no. 1 (2023): 849, <https://doi.org/10.1038/s41597-023-02598-x>.
38. L. Kaurani, R. Pradhan, S. Schröder, et al., “A Role for Astrocytic miR-129-5p in Frontotemporal Dementia,” *Translational Psychiatry* 15, no. 1 (2025): 142, <https://doi.org/10.1038/s41398-025-03338-y>.
39. Y. Wu, Y. G. Yao, and X. J. Luo, “SZDB: A Database for Schizophrenia Genetic Research,” *Schizophrenia Bulletin* 43, no. 2 (2017): 459–471.
40. W. Duan, Y.-P. Zhang, Z. Hou, et al., “Novel Insights Into NeuN: From Neuronal Marker to Splicing Regulator,” *Molecular Neurobiology* 53, no. 3 (2016): 1637–1647, <https://doi.org/10.1007/s12035-015-9122-5>.
41. H. Braak and E. Braak, “Evolution of the Neuropathology of Alzheimer’s Disease,” *Acta Neurologica Scandinavica* 94 (1996): 3–12, <https://doi.org/10.1111/j.1600-0404.1996.tb05866.x>.
42. M. C. Bridges, A. C. Daulagala, and A. Kourtidis, “Lncation: LncRNA Localization and Function,” *Journal of Cell Biology* 220, no. 2 (2021): 202009045, <https://doi.org/10.1083/jcb.202009045>.
43. F. Fasolo, H. Jin, G. Winski, et al., “Long Noncoding RNA MIAT Controls Advanced Atherosclerotic Lesion Formation and Plaque Destabilization,” *Circulation* 144, no. 19 (2021): 1567–1583, <https://doi.org/10.1161/CIRCULATIONAHA.120.052023>.
44. V. Feichtenschlager, L. Chen, Y. J. Zheng, et al., “The Therapeutically Actionable Long Non-Coding RNA ‘T-RECS’ is Essential to Cancer Cells’ Survival in NRAS/MAPK-Driven Melanoma,” *Molecular Cancer* 23, no. 1 (2024): 40, <https://doi.org/10.1186/s12943-024-01955-7>.
45. T. M. DeLorey, A. Handforth, S. G. Anagnostaras, et al., “Mice Lacking the  $\beta$ 3 Subunit of the GABAA Receptor Have the Epilepsy Phenotype and Many of the Behavioral Characteristics of Angelman Syndrome,” *The Journal of Neuroscience* 18 (1998): 8505–8514, <https://doi.org/10.1523/JNEUROSCI.18-20-08505.1998>.
46. J. W. Buckholtz, A. Meyer-Lindenberg, R. A. Honea, et al., “Allelic Variation in RGS4 Impacts Functional and Structural Connectivity in the Human Brain,” *The Journal of Neuroscience* 27, no. 7 (2007): 1584–1593, <https://doi.org/10.1523/JNEUROSCI.5112-06.2007>.
47. R. Gonzalez, K. Chávez-Pascacio, and A. Meneses, “Role of 5-HT5A Receptors in the Consolidation of Memory,” *Behavioural Brain Research* 252 (2013): 246–251.
48. L. Pini, M. Pievani, M. Bocchetta, et al., “Brain atrophy in Alzheimer’s Disease and Aging,” *Ageing Research Reviews* 30 (2016): 25–48, <https://doi.org/10.1016/j.arr.2016.01.002>.
49. A. P. Passaro, O. Aydin, M. T. A. Saif, and S. L. Stice, “Development of an Objective Index, Neural Activity Score (NAS), Reveals Neural Network Ontogeny and Treatment Effects on Microelectrode Arrays,” *Scientific Reports* 11, no. 1 (2021): 9110, <https://doi.org/10.1038/s41598-021-88675-w>.
50. A. Chopra, M. Xylaki, F. Yin, et al., “The epitranscriptomic m6A RNA Modification Modulates Synaptic Function in Ageing and in a Mouse Model of Synucleinopathy,” *bioRxiv* (2024).
51. S. Rumpel, J. LeDoux, A. Zador, and R. Malinow, “Postsynaptic Receptor Trafficking Underlying a Form of Associative Learning,” *Science* 308, no. 5718 (2005): 83–88, <https://doi.org/10.1126/science.1103944>.
52. E. Karran and B. De Strooper, “The Amyloid Hypothesis in Alzheimer Disease: New Insights From New Therapeutics,” *Nature Reviews Drug Discovery* 21, no. 4 (2022): 306–318, <https://doi.org/10.1038/s41573-022-00391-w>.
53. C. Chu, K. Qu, F. L. Zhong, S. E. Artandi, and H. Y. Chang, “Genomic Maps of Long Noncoding RNA Occupancy Reveal Principles of RNA-Chromatin Interactions,” *Molecular Cell* 44, no. 4 (2011): 667–678, <https://doi.org/10.1016/j.molcel.2011.08.027>.
54. T. Mondal, S. Subhash, R. Vaid, et al., “MEG3 Long Noncoding RNA Regulates the TGF- $\beta$  Pathway Genes Through Formation of RNA-DNA Triplex Structures,” *Nature Communications* 6 (2015): 7743.
55. A. K. Jain, Y. Xi, R. McCarthy, et al., “LncPRESS1 Is a p53-Regulated LncRNA that Safeguards Pluripotency by Disrupting SIRT6-Mediated Deacetylation of Histone H3K56,” *Molecular Cell* 64, no. 5 (2016): 967–981, <https://doi.org/10.1016/j.molcel.2016.10.039>.
56. M. Rosenberg, R. Blum, B. Kesner, et al., “Motif-driven Interactions Between RNA and PRC2 Are Rheostats That Regulate Transcription Elongation,” *Nature Structural & Molecular Biology* 28, no. 1 (2021): 103–117, <https://doi.org/10.1038/s41594-020-00535-9>.

57. S. Schröder, M. S. Sakib, D. M. Krüger, et al., “LncRNA 3222401L13Rik Is Upregulated in Aging Astrocytes and Regulates Neuronal Support Function through Interaction With Npas3,” *Non-Coding RNA* 11, no. 1 (2025): 2, <https://doi.org/10.3390/ncrna11010002>.
58. G. Q. C. Chen, Q. Zhang, B. Liu, and Q. Cui, “Genome-wide Analysis of human SNPs at Long Intergenic Noncoding RNAs,” *Human Mutation* 34, no. 2 (2013): 338–344, <https://doi.org/10.1002/humu.22239>.
59. R. Aguilar, M. Rosenberg, V. Levy, and J. T. Lee, “An Evolving Landscape of PRC2-RNA Interactions in Chromatin Regulation,” *Nature Reviews Molecular Cell Biology* 26, no. 8 (2025): 631–642.
60. M. von Schimmelmann, P. A. Feinberg, J. M. Sullivan, et al., “Polycomb Repressive Complex 2 (PRC2) Silences Genes Responsible for Neurodegeneration,” *Nature Neuroscience* 19, no. 10 (2016): 1321–1330, <https://doi.org/10.1038/nn.4360>.
61. L. Wu, P. Murat, D. Matak-Vinkovic, A. Murrell, and S. Balasubramanian, “Binding Interactions Between Long Noncoding RNA HOTAIR and PRC2 Proteins,” *Biochemistry* 52, no. 52 (2013): 9519–9527, <https://doi.org/10.1021/bi401085h>.
62. H. B. Cagirici, H. Budak, and T. Z. Sen, “G4Boost: A Machine Learning-based Tool for Quadruplex Identification and Stability Prediction,” *BMC Bioinformatics [Electronic Resource]* 23, no. 1 (2022): 240, <https://doi.org/10.1186/s12859-022-04782-z>.
63. H. Yu, F. Li, B. Yang, et al., “iM-Seeker: A Webserver for DNA i-motifs Prediction and Scoring via Automated Machine Learning,” *Nucleic Acids Research* 52, no. W1 (2024): W19–W28, <https://doi.org/10.1093/nar/gkae315>.
64. F. C. Kuo, M. J. Neville, R. Sabaratnam, et al., “HOTAIR Interacts With PRC2 Complex Regulating the Regional Preadipocyte Transcriptome and human Fat Distribution,” *Cell Reports* 40, no. 4 (2022): 111136, <https://doi.org/10.1016/j.celrep.2022.111136>.
65. C. C. Guo, C. H. Jiao, and Z. M. Gao, “Silencing of LncRNA BDNF-AS Attenuates A $\beta$ 25–35-Induced Neurotoxicity in PC12 Cells by Suppressing Cell Apoptosis and Oxidative Stress,” *Neurological Research* 40, no. 9 (2018): 795–804, <https://doi.org/10.1080/01616412.2018.1480921>.
66. Z. Lan, Y. Chen, J. Jin, Y. Xu, and X. Zhu, “Long Non-coding RNA: Insight into Mechanisms of Alzheimer’s Disease,” *Frontiers in Molecular Neuroscience* 14 (2022): 821002, <https://doi.org/10.3389/fnmol.2021.821002>.
67. J. L. Rinn, M. Kertesz, J. K. Wang, et al., “Functional Demarcation of Active and Silent Chromatin Domains in Human HOX Loci by Noncoding RNAs,” *Cell* 129, no. 7 (2007): 1311–1323, <https://doi.org/10.1016/j.cell.2007.05.022>.
68. M. C. Tsai, O. Manor, Y. Wan, et al., “Long Noncoding RNA as Modular Scaffold of Histone Modification Complexes,” *Science* 329, no. 5992 (2010): 689–693, <https://doi.org/10.1126/science.1192002>.
69. P. Poltronieri, “Regulatory RNAs: Role as Scaffolds Assembling Protein Complexes and their Epigenetic Deregulation,” *Exploration of Targeted Anti-Tumor Therapy* 5, no. 4 (2024): 841–876.
70. Y. Wu, Y. Liu, E. M. Levine, and M. S. Rao, “Hes1 but Not Hes5 Regulates an Astrocyte versus Oligodendrocyte Fate Choice in Glial Restricted Precursors,” *Developmental Dynamics* 226, no. 4 (2003): 675–689, <https://doi.org/10.1002/dvdy.10278>.
71. T. Ogata, T. Ueno, S. Hoshikawa, et al., “Hes1 functions Downstream of Growth Factors to Maintain Oligodendrocyte Lineage Cells in the Early Progenitor Stage,” *Neuroscience* 176 (2011): 132–141, <https://doi.org/10.1016/j.neuroscience.2010.12.015>.
72. H. Wang, L. Xu, C. Lai, et al., “Region-Specific Distribution of Olig2-expressing Astrocytes in Adult Mouse Brain and Spinal Cord,” *Molecular Brain* 14, no. 1 (2021): 36, <https://doi.org/10.1186/s13041-021-00747-0>.
73. L. M. Szweczyk, M. A. Lipiec, E. Liszewska, et al., “Astrocytic  $\beta$ -Catenin Signaling via TCF7L2 Regulates Synapse Development and Social Behavior,” *Molecular Psychiatry* 29, no. 1 (2024): 57–73, <https://doi.org/10.1038/s41380-023-02281-y>.
74. X. Cui, R. Zhang, Y. Yang, et al., “Identification and Characterization of Long Non-Coding RNA Carip in Modulating Spatial Learning and Memory,” *Cell Reports* 38, no. 8 (2022): 110398, <https://doi.org/10.1016/j.celrep.2022.110398>.
75. W. S. Liao, Q. Zhao, A. Bademosi, et al., “Fear Extinction Is Regulated by the Activity of Long Noncoding RNAs at the Synapse,” *Nature Communications* 14, no. 1 (2023): 7616, <https://doi.org/10.1038/s41467-023-43535-1>.
76. H. Li, L. Zheng, A. Jiang, Y. Mo, and Q. Gong, “Identification of the Biological Affection of Long Noncoding RNA BC200 in Alzheimer’s Disease,” *Neuroreport* 29, no. 13 (2018): 1061–1067, <https://doi.org/10.1097/WNR.0000000000001057>.
77. X. W. Yan, H. J. Liu, Y. X. Hong, T. Meng, J. Du, and C. Chang, “LncRNA XIST induces A $\beta$  accumulation and neuroinflammation by the epigenetic repression of NEP in Alzheimer’s disease,” *Journal of Neurogenetics* 36, no. 1 (2022): 11–20, <https://doi.org/10.1080/01677063.2022.2028784>.
78. L. Chakrabarti, T. K. Best, N. P. Cramer, et al., “Olig1 and Olig2 Triplication Causes Developmental Brain Defects in Down syndrome,” *Nature Neuroscience* 13, no. 8 (2010): 927–934, <https://doi.org/10.1038/nn.2600>.
79. B. Xu and C. Zheng, “Analysis of Long Noncoding RNAs-Related Regulatory Mechanisms in Duchenne Muscular Dystrophy Using a Disease-Related LncRNA-mRNA Pathway Network,” *Genetics Research* 2022 (2022): 8548804.
80. C. Kanach, J. K. Blusztajn, A. Fischer, I. Delalle, and D. MacBfAs, “MicroRNAs as Candidate Biomarkers for Alzheimer’s Disease,” *Noncoding RNA* 7, no. 1 (2021): 8, [10.3390/ncrna7010008](https://doi.org/10.3390/ncrna7010008).
81. D. M. Krüger, T. Pena, S. Liu, et al., “The Plasma miRNAome in ADNI: Signatures to Aid the Detection of at-Risk Individuals,” *Alzheimer’s & Dementia* 20, no. 11 (2024): 7479–7494.
82. S. Liu, T. Park, D. M. Krüger, et al., “Plasma miRNAs Across the Alzheimer’s Disease Continuum: Relationship to Central Biomarkers,” *Alzheimer’s & Dementia* 20, no. 11 (2024): 7698–7714.
83. M. Dibaj, M. Haghi, R. Safaralizadeh, and A. Saberi, “The Role of EZH2 and its Regulatory lncRNAs as a Serum-Based Biomarker in Alzheimer’s Disease,” *Molecular Biology Reports* 51, no. 1 (2024): 866, <https://doi.org/10.1007/s11033-024-09802-0>.
84. T. Wang, W. Zhang, J. M. A. Maclin, et al., “Novel Panel of Long Noncoding RNAs as Diagnostic Biomarkers for Amnesic Mild Cognitive Impairment in Peripheral Blood,” *Journal of Alzheimer’s Disease* 99, no. 4 (2024): 1385–1396, <https://doi.org/10.3233/JAD-231446>.
85. R. S. Finkel, E. Mercuri, B. T. Darras, et al., “Nusinersen versus Sham Control in Infantile-onset Spinal Muscular Atrophy,” *New England Journal of Medicine* 377, no. 18 (2017): 1723–1732.
86. T. M. Miller, M. E. Cudkovicz, A. Genge, et al., “Trial of Antisense Oligonucleotide Tofersen for SOD1 ALS,” *New England Journal of Medicine* 387, no. 12 (2022): 1099–1110, <https://doi.org/10.1056/NEJMoa2204705>.
87. M. S. Kariolis, R. C. Wells, J. A. Getz, et al., “Brain delivery of Therapeutic Proteins Using an Fc Fragment Blood-Brain Barrier Transport Vehicle in Mice and Monkeys,” *Science Translational Medicine* 12, no. 545 (2020): aay1359, <https://doi.org/10.1126/scitranslmed.aay1359>.
88. S. T. Crooke, X. H. Liang, B. F. Baker, and R. M. Crooke, “Antisense Technology: A Review,” *Journal of Biological Chemistry* 296 (2021): 100416, <https://doi.org/10.1016/j.jbc.2021.100416>.

## Supporting Information

Additional supporting information can be found online in the Supporting Information section.

**Supporting File 1:** advs74817-sup-0001-SuppMat.pdf.

**Supporting File 2:** advs74817-sup-0002-Tables.xlsx.